

# Novel insights on causes of disproportionate trends between particulate $\text{NO}_3^-$ and $\text{NO}_x$ emissions in Canadian urban atmospheres

Qinchu Fan<sup>1</sup>, Xiaohong Yao<sup>1,\*</sup>, Leiming Zhang<sup>2,\*</sup>

<sup>1</sup>Key Laboratory of Marine Environment and Ecology (MOE), and Frontiers Science Center for Deep Ocean Multispheres and Earth System, Sanya Oceanographic Institution, Ocean University of China, Qingdao 266100, China

<sup>2</sup>Air Quality Research Division, Science and Technology Branch, Environment and Climate Change Canada, Toronto, Ontario, M3H 5T4, Canada

\* Corresponding author: Xiaohong Yao (xhyao@ouc.edu.cn), Leiming Zhang ([leiming.zhang@ec.gc.ca](mailto:leiming.zhang@ec.gc.ca))

1 **Abstract.** Particulate nitrate ( $\text{NO}_3^-$ ) is a key target for air pollution control; however,  
2 its response to  $\text{NO}_x$  emission reductions remains uncertain, particularly in cold climates.  
3 This study assesses long-term trends in fine- and coarse-mode  $\text{NO}_3^-$  (f- $\text{NO}_3^-$  and c- $\text{NO}_3^-$   
4 ) from 1990 to 2019 across seven Canadian cities, using data from by the National Air  
5 Pollution Surveillance (NAPS) network. The analysis reveals disproportionate trends  
6 between  $\text{NO}_3^-$  and  $\text{NO}_x$  emissions nationwide. In Edmonton, annual mean f- $\text{NO}_3^-$   
7 decreased by approximately 60% between 2007 and 2019, while provincial  $\text{NO}_x$   
8 emissions declined by only 10–20%. Similar patterns were observed in five of the six  
9 other cities during the most recent decade. These disproportionate trends are attributed  
10 to reductions in primary f- $\text{NO}_3^-$  emissions, localized dispersion processes, and wind  
11 anomalies modulated by Arctic Oscillation. In contrast, all cities exhibited a temporary  
12 increase in f- $\text{NO}_3^-$  during 1998–2007, coinciding with early  $\text{NO}_x$  control measures and  
13 consistent with an unintended enhancement of primary f- $\text{NO}_3^-$  emissions formed within  
14 stationary combustion plumes. c- $\text{NO}_3^-$  was largely insensitive to  $\text{NO}_x$  reduction in most  
15 cities (except for Edmonton), with variability governed primarily by neutralization  
16 reactions with alkaline aerosols rather than by the availability of gaseous  $\text{HNO}_3$ . These  
17 findings provide insight into the weak or absent response of f- $\text{NO}_3^-$  to  $\text{NO}_x$  emission  
18 reductions observed globally, particularly in cold-climate regions.

19  
20 **Keywords:** particulate nitrate, primary nitrate emission, decadal trends,  $\text{NO}_x$  emission  
21 reduction

## 1 Introduction

Particulate nitrate ( $\text{NO}_3^-$ ) has been a central focus of pollution control strategies in the past several decades due to its impact on air quality, climate, and ecosystem health (Balamurugan et al., 2022; Bell et al., 2007; Chan et al., 2021; Cheng et al., 2024; Dabek-Zlotorzynska et al., 2011; Duce et al., 2008; Font et al., 2024; Harrison et al., 2022; Man et al., 2015; Pullokaran et al., 2024; Squizzato et al., 2018; Sun et al., 2025; Thunis et al., 2021; Wang et al., 2020; Zaveri et al., 2021; Zhai et al., 2021; Zhang et al., 2008; Zhou et al., 2022).  $\text{NO}_3^-$  impacts air quality because it is a major chemical component of particulate matter, particularly fine particles. Besides, photolysis of  $\text{NO}_3^-$  produces highly reactive oxidants, such as hydroxyl radicals, HOCl, and  $\text{Cl}_2$ , thereby enhancing atmospheric oxidation capacity (Chen et al., 2025; Gen et al., 2022; Peng et al., 2022).  $\text{NO}_3^-$  contributes to climatic effects directly through radiative forcing and indirectly through increasing cloud condensation nuclei (Drugé et al., 2019; Zaveri et al., 2021). For instance, a modeling study showed that nitrate aerosols contributed significantly to shortwave radiative cooling, reaching up to  $-5 \text{ W m}^{-2}$  on a regional scale under clear-sky condition and  $-0.8 \text{ W m}^{-2}$  on global average (Zaveri et al., 2021).  $\text{NH}_4\text{NO}_3$  formed from condensation of gaseous species of  $\text{NH}_3$  and  $\text{HNO}_3$  can rapidly grow to the sizes of cloud condensation nuclei in cold atmospheres (Höpfner et al., 2019; Wang et al., 2022; Zhu et al., 2014). Additionally,  $\text{NO}_3^-$  contributes to atmospheric nitrogen deposition, which has ecosystem implications (Bose et al., 2018; Iizuka et al., 2025), and it can even undergo long-range transport in the atmosphere and eventually deposit into oceans or remote continental regions (Iizuka et al., 2025; Jonson et al., 2022; Qi et al., 2018).

Given the significant reductions of  $\text{SO}_2$  emissions worldwide in the past four decades, the impacts of  $\text{NO}_3^-$  on air quality, climate, and ecosystem health have garnered increasing attention (Aas et al., 2019; Feng et al., 2020; Hand et al., 2024; Sun et al., 2018; Velazquez-Garcia et al., 2023; Wang et al., 2021; Zhai et al., 2021). Unlike sulfate ( $\text{SO}_4^{2-}$ ), which predominantly exists in fine particulate matter ( $\text{PM}_{2.5}$ ),  $\text{NO}_3^-$  exists in both fine- and coarse-mode particles (referred to as f- $\text{NO}_3^-$  and c- $\text{NO}_3^-$ ,

52 respectively). As a semi-volatile substance, the fine and coarse fractions of  $\text{NO}_3^-$  vary  
53 with season and location (Peng et al., 2024; Yao and Zhang, 2012a, b; Zhang et al.,  
54 2008) because its volatility and partitioning with its gaseous precursors are influenced  
55 by ambient meteorological and chemical conditions, including temperature (T), relative  
56 humidity (RH), and mixing ratios of  $\text{HNO}_3$  and  $\text{NH}_3$  (Guo et al., 2016; Huo et al., 2025;  
57 Seinfeld and Pandis, 2016; Yao et al., 2003). This complicates the response of f- $\text{NO}_3^-$   
58 and c- $\text{NO}_3^-$  to changes in  $\text{NO}_x$  emissions (Balamurugan et al., 2022; Chan et al., 2021;  
59 Huo et al., 2025; Thunis et al., 2021; Zhai et al., 2021). Additionally, reduced  $\text{NO}_x$   
60 emissions may enhance the formation of  $\text{N}_2\text{O}_5$  at nighttime, a product that can form f-  
61  $\text{NO}_3^-$  through secondary aerosol formation, thereby further influencing the response of  
62 f- $\text{NO}_3^-$  to emission reductions (Fan et al., 2020; Shah et al., 2018; Wang et al., 2023;  
63 Ward et al., 2025; Yan et al., 2023; Zhou et al., 2022). It has been reported that f- $\text{NO}_3^-$   
64 can form from condensable species in fresh stationary combustion plumes, followed by  
65 dispersion and evaporation under freezing ambient conditions (Shen et al., 2022;  
66 USEPA, 2017; Xiao et al., 2025; Yang et al., 2024). This mechanism has been largely  
67 overlooked in studies examining the response of  $\text{NO}_3^-$  to  $\text{NO}_x$  emission reductions,  
68 particularly in regions with prolonged cold seasons.

69

70 Canada is a nation experiencing long cold winters. Higher concentrations of f- $\text{NO}_3^-$   
71 were predominantly observed during cold winter seasons, except during large-scale  
72 wildfire events mostly occurring in warm seasons (Bari and Kindzierski, 2016a, b;  
73 Dabek-Zlotorzynska et al., 2011; Edgerton et al., 2020; Jeong et al., 2011; Wang et al.,  
74 2021). The contributions of primary and/or secondary sources to the elevated f- $\text{NO}_3^-$   
75 concentrations in Canadian cold atmospheres remain poorly understood. The primary  
76 emissions of f- $\text{NO}_3^-$  likely arise from two major processes: (i) the rapid formation of f-  
77  $\text{NO}_3^-$  through reactions between  $\text{HNO}_{3\text{gas}}$  and  $\text{NH}_{3\text{gas}}$  within the first few seconds after  
78 combustion plumes exit the stack outlet (or vehicle exhaust pipes) and undergo cooling;  
79 and (ii) the formation of f- $\text{NO}_3^-$  via the reaction  $2\text{NO}_2 + \text{H}_2\text{O} \rightarrow \text{HNO}_3 + \text{HNO}_2$  within  
80 droplets produced in fresh cooling combustion plumes, followed by  $\text{NH}_{3\text{gas}}$   
81 neutralization before these droplets evaporate into ambient aerosols. Note that the fresh

82 plumes contain extremely high concentrations of various air pollutants, enabling the  
83 occurrence of the above-mentioned reactions (Seinfeld and Pandis, 2016; Zhang et al.,  
84 2021; Zhang et al., 2023).

85

86 The aforementioned knowledge gap hinders our understanding of how changes in  
87 primary f-NO<sub>3</sub><sup>-</sup> emissions influence the annual-scale response of f-NO<sub>3</sub><sup>-</sup> to NO<sub>x</sub>  
88 emission reductions. This gap appears to be global rather than unique to Canada, as  
89 indicated by the brief review of particulate NO<sub>3</sub><sup>-</sup> trends and their responses to NO<sub>x</sub>  
90 emission reductions summarized in Text S1 of the Supporting Information (SI). Two  
91 key points emerge. (1) The limited number of trend studies on particulate NO<sub>3</sub><sup>-</sup> across  
92 Canada, including f-NO<sub>3</sub><sup>-</sup> and total NO<sub>3</sub><sup>-</sup> (= f-NO<sub>3</sub><sup>-</sup> + c-NO<sub>3</sub><sup>-</sup>) in suspended particles,  
93 suggest that long-term changes are neither spatially uniform nor monotonic. (2) The  
94 non-linear and sometimes counterintuitive response of particulate NO<sub>3</sub><sup>-</sup> to NO<sub>x</sub>  
95 emission controls has been widely reported in the United States, Europe, and China, yet  
96 the underlying drivers remain insufficiently constrained. Together, these cross-regional  
97 comparisons motivate a Canada-focused synthesis that explicitly evaluates the non-  
98 linear influences of co-evolving precursor emissions, gas-particle partitioning, and  
99 meteorological variability in interpreting long-term f-NO<sub>3</sub><sup>-</sup> trends.

100

101 Additionally, significant decreases in NO<sub>x</sub> emissions across Canada mainly occurred  
102 between 1998 and 2008, with slight time shifting across different provinces (ECCC,  
103 2021). PM<sub>2.5</sub> speciation data since 2003 alone may not fully elucidate the response of  
104 NO<sub>3</sub><sup>-</sup> to reduced NO<sub>x</sub> emissions. Fortunately, both f-NO<sub>3</sub><sup>-</sup> and c-NO<sub>3</sub><sup>-</sup> data are available  
105 from the National Air Pollution Surveillance (NAPS) at 12 urban sites (Dabek-  
106 Zlotorzynska et al., 2011; Dabek-Zlotorzynska et al., 2019). Seven of these 12 sites  
107 have integrated measurements of particulate chemical components spanning 1-3  
108 decades, enabling the examination of long-term trends in f-NO<sub>3</sub><sup>-</sup> and c-NO<sub>3</sub><sup>-</sup> in  
109 Canadian urban atmospheres and their responses to reduced NO<sub>x</sub> emissions.

110

111 In this study we investigated long-term trends in the annual average mass  
112 concentrations of f-NO<sub>3</sub><sup>-</sup> and c-NO<sub>3</sub><sup>-</sup> in Canadian urban atmospheres, with a particular  
113 focus on the responses of f-NO<sub>3</sub><sup>-</sup> and c-NO<sub>3</sub><sup>-</sup> to NO<sub>x</sub> emission reductions since 1990  
114 and the associated mechanisms. The analyses are structured into three major parts: Part  
115 1 examines the long-term trends of f-NO<sub>3</sub><sup>-</sup> and c-NO<sub>3</sub><sup>-</sup>, firstly in Edmonton (Section  
116 3.1) and then extended the other six cities (Sections 3.2 and 3.3); Part 2 investigates the  
117 key factors influencing f-NO<sub>3</sub><sup>-</sup> levels in Edmonton (Section 3.4) and the role of primary  
118 f-NO<sub>3</sub><sup>-</sup> emissions in shaping these trends (Section 3.5); and Part 3 provides a  
119 comprehensive assessment of uncertainties associated with f-NO<sub>3</sub><sup>-</sup> and their potential  
120 impact on the observed trends (Section 3.6). Finally, a summary of the major findings  
121 and potential implications are presented in Section 4.

## 122 **2 Methodology**

### 123 **2.1 Monitoring sites and data sources**

124 The present study utilized long-term data monitored at two urban sites in Edmonton (S-  
125 90132, Latitude: 53.486, Longitude: -113.465; and S-90130, Latitude: 53.544,  
126 Longitude: -113.499), as well as one urban site in each of the other six cities, including  
127 Winnipeg (49.898, -97.147), Victoria (48.442, -123.363), Vancouver (49.281, -  
128 122.849), Montreal (45.543, -75.572), Quebec City (46.821, -71.221), and Hamilton  
129 (45.258, -79.862) (Figures S1 and S2). The first four cities are in western Canada with  
130 Edmonton in the province of Alberta, Winnipeg in the province of Manitoba, and  
131 Victoria and Vancouver in the province of British Columbia. The other three cities are  
132 in eastern Canada with Montreal and Quebec City in the province of Quebec and  
133 Hamilton in the province of Ontario.

134

135 In Edmonton, at the S-90132 site speciation PM<sub>2.5</sub> samplers have been used since 2007  
136 to measure mass concentrations of PM<sub>2.5</sub>, ionic concentrations in PM<sub>2.5</sub>, and the levels  
137 of acidic and alkaline gases, with 24-h integrated sampling occurring one in every three  
138 days (Bari and Kindzierski, 2016a, b). At the S-90130 site, ionic species, including

139  $\text{NO}_3^-$ ,  $\text{SO}_4^{2-}$ ,  $\text{NH}_4^+$ ,  $\text{Na}^+$ , and various elements in both  $\text{PM}_{2.5}$  and  $\text{PM}_{2.5-10}$  were collected  
140 using Dichotomous Air Samplers (Thermo, US), with 24-h integrated sampling  
141 occurring one in every six days during 1986-2005. Since no emission data were  
142 available before 1990, only the data after 1990 were included in this study. The ionic  
143 data were missing in 2006 at both sites. Note that the identical Dichotomous Air  
144 Samplers were also used at S-90132 for several years to collect  $\text{PM}_{2.5}$ , though no ionic  
145 data, for comparison purpose. Both datasets were included because neither alone covers  
146 the primary  $\text{NO}_x$  mitigation period in Edmonton.

147

148 In Hamilton, an identical speciation sampler has been used since 2013 to measure ionic  
149 components in  $\text{PM}_{2.5}$  and gases, with sampling occurring one in every three days. In  
150 this city, only elements have been measured in samples collected by the Dichotomous  
151 Air Sampler since then. At the other five urban sites selected for this study, speciation  
152  $\text{PM}_{2.5}$  data were either unavailable (Winnipeg and Quebec City) or collected one in  
153 every six days after 2005 (Victoria, Vancouver, and Montreal).  $\text{PM}_{2.5}$  air samplers  
154 (Thermo, US) were used in Victoria and Winnipeg after 2012, and  $\text{PM}_{2.5}$  samplers  
155 (TISCH, US) were used in Vancouver and Montreal after 2016. Corresponding  $\text{NO}_3^-$   
156 data in  $\text{PM}_{2.5-10}$  were not available at these sites since then. In this study,  $\text{NO}_3^-$  in  $\text{PM}_{2.5}$   
157 collected by speciation samplers was also referred to as f- $\text{NO}_3^-$ . The same definition is  
158 applied to f- $\text{SO}_4^{2-}$  and f- $\text{NH}_4^+$ , which were used to facilitate the analysis of f- $\text{NO}_3^-$ .

159

160 Hourly average mass concentrations of  $\text{PM}_{2.5}$  and mixing ratios of  $\text{NO}_2$  were also  
161 routinely measured at each site, except that no  $\text{NO}_2$  mixing ratios were reported at S-  
162 90132. In this case, the values from S-90130 were used in this study. For certain parts  
163 of the year at the sites in Victoria and Quebec City,  $\text{NO}_2$  mixing ratios were also  
164 unavailable. In these cases, the mixing ratios of  $\text{NO}_2$  measured at different sites within  
165 a 1-2 km radius in the same city were used to facilitate the analysis. All the data are  
166 publicly available through the National Air Pollution Surveillance (NAPS) program  
167 network ([https://data-donnees.ec.gc.ca/data/air/monitor/national-air-pollution-](https://data-donnees.ec.gc.ca/data/air/monitor/national-air-pollution-surveillance-naps-program/?lang=en)  
168 [surveillance-naps-program/?lang=en](https://data-donnees.ec.gc.ca/data/air/monitor/national-air-pollution-surveillance-naps-program/?lang=en)) and summarized in Table S1.

169

170 NO<sub>x</sub>, SO<sub>2</sub>, and NH<sub>3</sub> emissions data at the provincial level in Canada were obtained from  
171 [https://www.canada.ca/en/environment-climate-change/services/environmental-  
173 indicators/air-pollutant-emissions.html](https://www.canada.ca/en/environment-climate-change/services/environmental-<br/>172 indicators/air-pollutant-emissions.html). The monthly average wind fields were  
174 downloaded from <https://psl.noaa.gov/data/gridded/data.narr.html> (Figures 1 and S1),  
175 and the Arctic Oscillation (AO) Indexes were obtained from  
176 <https://www.ncdc.noaa.gov/teleconnections/ao/> (Figure S1d). Ground-level  
177 meteorological data from the airports of these cities were also downloaded from  
178 <https://www.wunderground.com/about/data>.

178

179 It should be noted that existing techniques for measuring ambient HNO<sub>3gas</sub> are subject  
180 to certain artifacts. Specifically, the Na<sub>2</sub>CO<sub>3</sub>-coated denuder used in speciation  
181 samplers is designed to remove acidic gases upstream of PM<sub>2.5</sub> collection on a Teflon  
182 filter, thereby minimizing positive artifacts in the collected PM<sub>2.5</sub> (Dabek-Zlotorzynska  
183 et al., 2011, 2019). However, measurements obtained using the denuder technique do  
184 not exclusively represent HNO<sub>3gas</sub>. Instead, they include HNO<sub>3gas</sub>, N<sub>2</sub>O<sub>5gas</sub>, and other  
185 acidic gases that react with Na<sub>2</sub>CO<sub>3</sub> to form NaNO<sub>3</sub>. Consequently, the reported  
186 concentrations reflect an upper bound of (HNO<sub>3gas</sub> + N<sub>2</sub>O<sub>5gas</sub>). To avoid ambiguity, the  
187 measured values are denoted as HNO<sub>3gas</sub>\* rather than HNO<sub>3gas</sub> throughout the following  
188 discussion. Importantly, this measurement uncertainty does not materially affect the  
189 conclusions of the present study, as HNO<sub>3gas</sub>\* concentrations remain substantially lower  
190 than the corresponding particulate nitrate levels during the high-nitrate winter periods  
191 examined here (see Section 3.4). Nevertheless, the upper-bound nature of HNO<sub>3gas</sub>\*  
192 may introduce bias in gas–particle equilibrium analyses, particularly during winter  
193 nighttime high-concentration episodes, when the true HNO<sub>3gas</sub> mixing ratio may be  
194 considerably lower than HNO<sub>3gas</sub>\* due to a potentially substantial contribution from  
195 N<sub>2</sub>O<sub>5gas</sub>.

## 196 2.2 Statistical analysis

197 Annual average mass concentrations of f-NO<sub>3</sub><sup>-</sup> and c-NO<sub>3</sub><sup>-</sup> were calculated from all  
198 available data in each calendar year. However, data loss was common in each city and  
199 year despite sampling occurring one in every three or six days. To minimize uncertainty  
200 from data loss and ensure sufficient data for trend analysis, data for trend analysis were  
201 excluded for any year when measurements for two consecutive months were  
202 unavailable. To analyze the time series of the annual average mass concentrations of  
203 each species, the Mann-Kendall (M-K) analysis was employed. The qualitative trend  
204 results determined by the M-K method include: (i) an increasing/decreasing trend with  
205 a *P* value of <0.05, (ii) a probable increasing/decreasing trend with a *P* value between  
206 0.05 and 0.1, (iii) a stable trend with a *P* value >0.1, as well as a ratio of <1.0 between  
207 the standard deviation and the mean of the dataset, and (iv) a no trend with a *P* >0.1 and  
208 other conditions (Lin et al., 2022).

209

210 To quantify the overall effect of climate anomalies on the annual average f-NO<sub>3</sub><sup>-</sup>  
211 between a pair of two years, our recently developed identical-percentile regression  
212 analysis was used (Lin et al., 2022; Yao and Zhang, 2024). In this method, the data  
213 sizes of the paired two-year should be the same (e.g., with the same time resolution and  
214 filling up all the missing data). The two sets of data, originally in time series, are sorted  
215 separately from the smallest to the largest to generate two percentile-based data arrays,  
216 which were then used for regression analysis with the intercept being set to be zero.  
217 The regression analysis can also be conducted using data in any particular percentile  
218 range for exploring different research targets. If the data sizes of the paired two-year  
219 are different, the one with a larger size can be modified to match the one with a smaller  
220 size using the method presented by Lin et al. (2022) and Yao and Zhang (2024) before  
221 applying the regression analysis described above. Moreover, a Random Forest (RF)  
222 model was employed to evaluate the relative importance of meteorological and seasonal  
223 timing variables in driving f-NO<sub>3</sub><sup>-</sup> formation (Text S2 of SI), and the Flexible 0-D

224 Atmospheric Model (F0AM) was applied to simulate secondary production of f-NO<sub>3</sub><sup>-</sup>  
225 (Text S3 of SI).

## 226 **3 Results and discussion**

### 227 **3.1 Complexity of particulate nitrate trends in urban atmosphere of Edmonton**

228 As mentioned in Section 2.1, two sites (S-90130 and S-90132) in Edmonton were  
229 selected for investigation due to the discontinued data coverage at both sites. Annual  
230 average mass concentrations of f-NO<sub>3</sub><sup>-</sup> at S-90130 from 1990 to 2005 and at S-90132  
231 from 2007 to 2019 were analyzed to illustrate the complexity of particulate nitrate  
232 trends in the urban atmosphere (Figure 1a). As mentioned in Section 2.1, data in 2006  
233 were missing at both sites. For comparison, annual average mass concentrations of c-  
234 NO<sub>3</sub><sup>-</sup> at S-90130 from 1990 to 2005 are also shown in Figure 1a and those of f-NH<sub>4</sub><sup>+</sup>  
235 and f-SO<sub>4</sub><sup>2-</sup> at S-90130 and S-90132 from 1990 to 2019 are shown in Figure S3. To  
236 facilitate analysis, annual average mixing ratios of NO<sub>2</sub> at S-90130 from 1995 to 2019  
237 are shown in Figure 1b, and annual provincial total emissions of NO<sub>x</sub>, SO<sub>2</sub>, and NH<sub>3</sub> in  
238 Alberta are also presented (Figures 1b, S3a and S3c, respectively). Correlation analyses  
239 between f-NO<sub>3</sub><sup>-</sup> (or c-NO<sub>3</sub><sup>-</sup>) and provincial total emissions of NO<sub>x</sub> in 1990-2005 and  
240 between f-SO<sub>4</sub><sup>2-</sup> and provincial total emissions of SO<sub>2</sub> in 1990-2019 are conducted  
241 (Figures 1c and S3b, respectively).

242

243 At S-90130, annual average f-NO<sub>3</sub><sup>-</sup> and c-NO<sub>3</sub><sup>-</sup> was  $0.48 \pm 0.25 \mu\text{g m}^{-3}$  (average  $\pm$   
244 standard deviation) and  $0.15 \pm 0.05 \mu\text{g m}^{-3}$ , respectively, during 1990 - 2005. No trend  
245 or stable trend was found for these species ( $P > 0.10$ ), likely due to a bell-shaped change  
246 in provincial total NO<sub>x</sub> emissions from 1990 to 2005. In fact, a significant correlation  
247 was found between annual average c-NO<sub>3</sub><sup>-</sup> and provincial total NO<sub>x</sub> emissions during  
248 1990-2005 ( $P < 0.01$ ). However, a significant correlation between annual average f-  
249 NO<sub>3</sub><sup>-</sup> and provincial NO<sub>x</sub> emissions was obtained only during 1992-2005 ( $P < 0.01$ ),  
250 but not for the entire period during 1990-2005 with the values in 1990-1991 being  
251 substantially deviating from the regression curve. Such a deviation is yet to be

252 explained. Notably,  $f\text{-NO}_3^-$  and  $c\text{-NO}_3^-$  were not significantly correlated in any  
253 individual year during 1990–2005 ( $R^2 < 0.1$ ;  $P > 0.05$ ). The same pattern was observed  
254 at the other six sites analyzed in this study. The lack of correlation between  $f\text{-NO}_3^-$  and  
255  $c\text{-NO}_3^-$  is discussed in detail in Section 3.2.

256

257 At S-90132, annual average  $f\text{-NO}_3^-$  was  $1.3 \pm 0.40 \mu\text{g m}^{-3}$  during 2007 - 2019.  $f\text{-NO}_3^-$   
258 exhibited a decreasing trend ( $P < 0.01$ ), with a Sen's Slope of  $0.063 \mu\text{g m}^{-3} \text{ yr}^{-1}$ ,  
259 resulting in an overall decrease of approximately 60% during this period. In  
260 comparison, the monitored  $\text{NO}_2$  mixing ratios at a different site (S-90130) decreased by  
261 approximately 20%, while provincial total  $\text{NO}_x$  emissions in Alberta were reduced by  
262 only ~10% during the same period. Such disproportionate decreases were also  
263 identified for both  $f\text{-NO}_3^-$  and  $c\text{-NO}_3^-$  at S-90130 in the selected period of 1997-2005,  
264 with a ~60% decrease in their annual average concentrations compared to a ~20%  
265 decrease in both the  $\text{NO}_2$  mixing ratios and provincial  $\text{NO}_x$  total emissions. Notably,  
266  $\text{NO}_2$  mixing ratios at the urban site were significantly correlated with Alberta's total  
267 provincial  $\text{NO}_x$  emissions, with  $R^2 = 0.81$  over 1997–2019 ( $P < 0.01$ ) and a slightly  
268 weaker correlation ( $R^2 = 0.57$ ) over the shorter period of 2007–2019 ( $P < 0.01$ ). These  
269 results indicate broadly consistent  $\text{NO}_x$  mitigation signals at both the provincial and city  
270 scales. Thus, the disproportionate large decrease in the annual average  $f\text{-NO}_3^-$  at S-  
271 90132 relative to the reduction in provincial  $\text{NO}_x$  emissions is analyzed below by  
272 considering major driving factors (Section 3.4), primary and secondary sources  
273 (Section 3.5), and potential uncertainties in the data of the generated annual average  $f\text{-}$   
274  $\text{NO}_3^-$  (Sections 3.6). It should be noted that the annual average  $f\text{-NO}_3^-$  measured at S-  
275 90132 in 2007-2019 were significantly higher than those recorded at S-90130 in 1990-  
276 2005 ( $P < 0.01$ ), which could be attributed to an unexpected mitigation effect, as  
277 analyzed in Section 3.3 below.

278

279 Unlike  $f\text{-NO}_3^-$ , annual average  $f\text{-SO}_4^{2-}$  exhibited a relatively smooth decreasing trend  
280 ( $P < 0.01$ ), with a Sen's slope of  $0.029 \mu\text{g m}^{-3} \text{ yr}^{-1}$  if combining data at S-90130 from  
281 1990 to 2005 and at S-90132 from 2007 to 2019 together (Figure S3a). This trend was

282 mostly consistent with a  $0.021 \mu\text{g m}^{-3} \text{yr}^{-1}$  decrease in the provincial total  $\text{SO}_2$  emissions  
283 from 1990 to 2019. Additionally, a moderately strong correlation was found between  
284 the annual average  $\text{f-SO}_4^{2-}$  and the provincial total  $\text{SO}_2$  emissions over the three decades  
285 ( $P < 0.01$ , Figure S3b). The  $\text{f-SO}_4^{2-}$  trend in the urban atmosphere reflects the mitigation  
286 effect, as has also been reported for rural atmospheres in Canada (Cheng and Zhang,  
287 2017; Feng et al., 2020).  $\text{f-SO}_4^{2-}$ , typically formed through in-cloud aqueous reactions  
288 and with non-volatile properties, is generally associated with regional sources, and thus  
289 tends to be spatially homogeneously distributed in urban scales (Bell et al., 2007; He et  
290 al., 2001; Park et al., 2004). This may explain the much smaller gaps in the annual  
291 average  $\text{f-SO}_4^{2-}$  between the two nearby urban sites, as compared to the case of  $\text{f-NO}_3^-$   
292 .

293  
294 Annual average  $\text{f-NH}_4^+$  exhibited a decreasing trend ( $P < 0.05$ ) if combining data at S-  
295 90130 from 1990 to 2005 and at S-90132 from 2007 to 2019 (Figure S3c). However,  
296 the trend was stable at both sites during the two separate periods ( $P > 0.10$ ). From 1990  
297 to 2019, the provincial total  $\text{NH}_3$  emissions increased by approximately 40% (Figure  
298 S3c). The phenomenon of the decoupled trends between  $\text{f-NH}_4^+$  and  $\text{NH}_3$  emissions  
299 widely occurred in Canada and the U.S. in the recent decades, as reported in Yao and  
300 Zhang (2019). This is because the level of  $\text{f-NH}_4^+$  was mainly controlled by those of  
301  $\text{SO}_4^{2-}$  and  $\text{NO}_3^-$  through neutralization reactions, especially under  $\text{NH}_3$ -rich conditions  
302 (Bari and Kindzierski, 2016b; Dabek-Zlotorzynska et al., 2011; Edgerton et al., 2020).  
303 The equivalent ratios of  $\text{NH}_4^+$  to  $(\text{SO}_4^{2-} + \text{NO}_3^-)$  in two selected years support this  
304 hypothesis (Figure S4).

### 305 **3.2 Trends of $\text{f-NO}_3^-$ and $\text{c-NO}_3^-$ in urban atmospheres of Winnipeg – an inland** 306 **city in western Canada**

307 The annual average  $\text{f-NO}_3^-$  in Winnipeg varied within a range of  $0.07\text{-}0.70 \mu\text{g m}^{-3}$ , with  
308 a long-term average of  $0.32 \pm 0.15 \mu\text{g m}^{-3}$  from 1990 to 2018. A stable trend in annual  
309 average  $\text{f-NO}_3^-$  was identified by the M-K method ( $P = 0.51$ ; Figure 1d). The annual  
310 average  $\text{c-NO}_3^-$  varied within an even smaller range of  $0.13\text{-}0.29 \mu\text{g m}^{-3}$ , with a long-

311 term average of  $0.19 \pm 0.04 \mu\text{g m}^{-3}$  during 1990–2012. A probable increasing trend in  
312 annual average c-NO<sub>3</sub><sup>-</sup> was identified ( $P = 0.06$ ). Over the same period, both the annual  
313 average mixing ratio of NO<sub>2</sub> at this site and provincial total NO<sub>x</sub> emissions in Manitoba  
314 exhibited decreasing trends ( $P < 0.01$ ) (Figure 1e), and they correlated with each other  
315 strongly ( $R^2 = 0.90$ ,  $P < 0.01$ ). The absence of a corresponding decrease in f-NO<sub>3</sub><sup>-</sup>  
316 concentration compared to NO<sub>x</sub> emissions is likely attributable to enhanced primary  
317 emissions of f-NO<sub>3</sub><sup>-</sup>-containing aerosols, as discussed in Sections 3.3 and 3.5 below.  
318 This is clearly supported by the following evidence: from 1999 to 2004, annual average  
319 f-NO<sub>3</sub><sup>-</sup> increased by approximately 200%, even as provincial NO<sub>x</sub> emissions and NO<sub>2</sub>  
320 mixing ratios declined by about 10%. Accordingly, the trend in f-NO<sub>3</sub><sup>-</sup> concentrations  
321 was analyzed in two separate periods: 1990–2002 and 2003–2018. The year of 2003 is  
322 allocated into the second rather than the first period based on the curve of annual  
323 variation shown in Figure 1d. In the first period (1990–2002), f-NO<sub>3</sub><sup>-</sup> showed a probable  
324 decreasing trend, with a Sen's Slope of  $0.017 \mu\text{g m}^{-3} \text{ year}^{-1}$  and a total decline of about  
325 80%. This sharp decrease cannot be explained by the relatively modest 10–20%  
326 reductions in NO<sub>2</sub> and NO<sub>x</sub> during the same period, suggesting that highly localized  
327 factors and/or uncertainties caused by coarse resolution data (1 in every 6 days) were  
328 likely the dominant contributors. The related uncertainty analysis is presented in  
329 Section 3.6 below. In the second period (2003–2018), f-NO<sub>3</sub><sup>-</sup> exhibited a decreasing  
330 trend with a Sen's Slope of  $0.018 \mu\text{g m}^{-3} \text{ year}^{-1}$ , amounting to an overall reduction of  
331 approximately 70%, which also exceeded the ~50% reduction in NO<sub>2</sub> mixing ratios at  
332 the same site and the ~30% reduction in provincial NO<sub>x</sub> emissions. The  
333 disproportionate trends between f-NO<sub>3</sub><sup>-</sup> and NO<sub>x</sub> emissions observed in Winnipeg are  
334 similar to the case in Edmonton discussed above.

335

336 When the time series of daily concentrations of f-NO<sub>3</sub><sup>-</sup> and c-NO<sub>3</sub><sup>-</sup> were examined for  
337 a low-concentration year (1996) and a high-concentration year (2007) (Figure 1f-g),  
338 elevated concentrations of f-NO<sub>3</sub><sup>-</sup> were predominantly observed during the cold  
339 months. High concentrations of f-NO<sub>3</sub><sup>-</sup> were likely from primary sources, as discussed  
340 in Section 3.5 below, considering the similar climate in inland western Canada. This,

341 however, needs to be confirmed using  $\text{HNO}_{3\text{gas}}^*$  data, which are not available at this  
342 site. In contrast, elevated concentrations of  $\text{c-NO}_3^-$  typically occurred during warmer  
343 months. Again, no significant correlation was observed between  $\text{f-NO}_3^-$  and  $\text{c-NO}_3^-$  in  
344 any year ( $R^2 < 0.1$ ,  $P > 0.05$ ). Given the probable increasing trend in annual average  $\text{c-}$   
345  $\text{NO}_3^-$  despite decreasing  $\text{NO}_x$  emissions at both city and provincial scales, and  
346 considering the seasonal pattern of elevated levels, it is likely that the trend in  $\text{c-NO}_3^-$   
347 was governed by the availability of alkali aerosols associated with suspended road dust  
348 and road-salt particles capable of neutralizing  $\text{HNO}_{3\text{gas}}^*$ , rather than by changes in  
349  $\text{HNO}_{3\text{gas}}^*$  itself. As further illustrated in Section 3.4 below for the case of Edmonton,  
350 stagnant winter meteorological conditions did not coincide with elevated  $\text{HNO}_{3\text{gas}}^*$   
351 concentrations, likely due to the accompanying sub-freezing temperatures. Moreover,  
352 stagnant and freezing conditions are not conducive to the suspension of road dust and  
353 road-salt particles during winter. This interpretation is also supported by findings  
354 reported in literature at rural sites in Canada (Cheng and Zhang, 2017; Feng et al., 2020)  
355 and urban and rural sites in the U.S. (Sickles II and Shadwick, 2015) and U.K. (Tang et  
356 al., 2018), where positive correlations between  $\text{HNO}_{3\text{gas}}^*$  and  $\text{NO}_2$  have been observed,  
357 suggesting that a reduction in  $\text{NO}_x$  would not typically lead to enhanced  $\text{HNO}_{3\text{gas}}^*$   
358 formation.

### 359 **3.3 Time window for unintended effects of $\text{NO}_x$ mitigation on $\text{f-NO}_3^-$ aerosols in** 360 **Canadian urban atmospheres and associated shaped trends of $\text{f-NO}_3^-$ and $\text{c-NO}_3^-$**

361 Long-term trends of  $\text{f-NO}_3^-$  could be distorted by unintentionally increased  $\text{f-NO}_3^-$   
362 primary emissions resulted from certain  $\text{NO}_x$  mitigation measures. Such phenomena  
363 were repeatedly observed in urban atmospheres across Canada during a consistent time  
364 window from approximately 1998 to 2007, as illustrated in Figures 1, and S5 as well as  
365 those aforementioned in Edmonton and Winnipeg. During this period, similar  $\text{NO}_x$   
366 mitigation actions were taken in both Canada and the U.S., regulated by the Canada -  
367 U.S. Air Quality Agreement signed in 1991 and further expanded in 2000. Although  
368 mitigation policies were likely implemented independently in each province in Canada,  
369 and the exact timing may have varied slightly, a consistent pattern emerged. For

370 example, in the province of Quebec, the annual average f-NO<sub>3</sub><sup>-</sup> increased by  
371 approximately 150% in Quebec City from 1998 to 2003 and by around 300% in  
372 Montreal from 1998 to 2002. During the same period, annual average mixing ratio of  
373 NO<sub>2</sub> decreased by approximately 10% in both cities, while provincial total NO<sub>x</sub>  
374 emissions remained nearly unchanged. In the province of Ontario, annual average f-  
375 NO<sub>3</sub><sup>-</sup> in Hamilton remained relatively low at 0.69 ± 0.09 µg m<sup>-3</sup> during 1995–1999, but  
376 rose sharply to 1.6 µg m<sup>-3</sup> in 2001, with a notable dip to 0.85 µg m<sup>-3</sup> in 2002 possibly  
377 due to climate anomaly, bounced back to 1.7 µg m<sup>-3</sup> in 2004 and stabilized at 1.6 µg m<sup>-3</sup>  
378 in 2005. During the period from 1999 - 2005, both observed NO<sub>2</sub> mixing ratios in  
379 Hamilton and provincial NO<sub>x</sub> emissions in Ontario began to decline by 20–30%. A  
380 similar pattern was also found in western coastal urban areas such as Victoria and  
381 Vancouver, both located in British Columbia, between 1998 and 2002 (Figure 2), where  
382 annual average f-NO<sub>3</sub><sup>-</sup> increased by approximately 100% while NO<sub>2</sub> mixing ratios and  
383 provincial NO<sub>x</sub> emissions declined by 10–30%. These widespread, disproportionate  
384 trends between f-NO<sub>3</sub><sup>-</sup> and NO<sub>x</sub> emissions across multiple cities strongly suggest that,  
385 during this early control window, NO<sub>x</sub> mitigation measures may have been  
386 accompanied by an unintended increase in primary f-NO<sub>3</sub><sup>-</sup> emissions, potentially  
387 associated with condensable particulate matter (CPM) and/or by-products of emission  
388 control technologies. However, no direct facility measurement data were made 20-year  
389 ago to verify this hypothesis. In fact, the USEPA only issued the method protocol for  
390 determining condensable particulate matter in 2017. Evidence from recent studies in  
391 developing countries further indicates that early-stage NO<sub>x</sub> controls (e.g., NH<sub>3</sub>-SCR  
392 operated at >300 °C) can be susceptible to imperfect ammonia dosing and the formation  
393 of associated by-products (Yang et al., 2016). This provides a plausible mechanistic  
394 explanation, although the specific causes in Canada and the United States cannot be  
395 definitively determined in the absence of historical CPM measurements. Accordingly,  
396 trend analysis of particulate nitrate should treat this period separately, with a  
397 demarcation line drawn at approximately 2002 or later.

398

399 In contrast to this early-phase behavior, several lines of evidence suggest that primary  
400 f-NO<sub>3</sub><sup>-</sup> emissions have likely declined in recent years. At the national scale, Canada's  
401 electricity supply has shifted markedly toward CO<sub>2</sub>-emission-free sources (now  
402 exceeding 80%), which are also largely free of NO<sub>x</sub> emissions. This transition should  
403 reduce primary nitrate-related emissions from the power sector (Canada Electricity  
404 Advisory Council, 2024). In addition, the rapidly increasing share of zero-emission  
405 vehicles, accounting for 10.8% of new vehicle registrations in 2023, is expected to  
406 further decrease primary f-NO<sub>3</sub><sup>-</sup> emissions from the transportation sector (Statistics  
407 Canada, 2024). Consistent with these broader trends, observations in Edmonton show  
408 that the decline in annual mean f-NO<sub>3</sub><sup>-</sup> concentrations over the past decade has been  
409 substantially larger than the corresponding decrease in NO<sub>2</sub>. This divergence supports  
410 the interpretation that reductions in primary f-NO<sub>3</sub><sup>-</sup> emissions have likely been an  
411 important contributing factor.

412

413 Setting the demarcation line at 2003 in Quebec City (noting the substantial data loss in  
414 2002 for this city) and at 2002 in Montreal, the annual average f-NO<sub>3</sub><sup>-</sup> decreased by  
415 more than 70% over the subsequent 16- or 17-year period, largely agree with the 40-  
416 60% reductions in NO<sub>2</sub> mixing ratios and provincial NO<sub>x</sub> emissions during the same  
417 period. The slight differences in their decreasing rates could be attributed to unintended  
418 changes in primary emissions of f-NO<sub>3</sub> aerosols as discussed above, non-linear  
419 atmospheric chemistry process involving other chemical species, and data uncertainties,  
420 etc. Notably, the annual average c-NO<sub>3</sub><sup>-</sup> showed no significant trend during these  
421 periods in either city, suggesting that c-NO<sub>3</sub><sup>-</sup> levels may have been more strongly  
422 influenced by the presence of alkali aerosols capable of neutralizing HNO<sub>3gas</sub><sup>\*</sup> rather  
423 than by the availability of HNO<sub>3gas</sub><sup>\*</sup> itself. Data prior to 2002 (Montreal) or 2003  
424 (Quebec City) were insufficient in duration to support robust trend analysis;  
425 nevertheless, the influence of unintended mitigation effects during this period was still  
426 evident. In comparison, if removing the demarcation line and considering the whole  
427 data record together, annual average f-NO<sub>3</sub><sup>-</sup> would show no clear trend from 1995 to  
428 2018 in Quebec City and a stable trend from 1997 to 2018 in Montreal. Over the full

429 period, annual average f-NO<sub>3</sub><sup>-</sup> and c-NO<sub>3</sub><sup>-</sup> were 0.41 ± 0.19 µg m<sup>-3</sup> and 0.19 ± 0.05 µg  
430 m<sup>-3</sup>, respectively, in Quebec City and 0.57 ± 0.38 µg m<sup>-3</sup> and 0.28 ± 0.06 µg m<sup>-3</sup>,  
431 respectively, in Montreal.

432

433 Similarly, if setting a demarcation line at the year of 2002 for Victoria and Vancouver,  
434 f-NO<sub>3</sub><sup>-</sup> would show either a significant decreasing trend or a probable decreasing trend,  
435 with a total decrease of around 40% in both cities from 2002 to 2018. These declines  
436 were broadly consistent with the 30–40% decreases in both NO<sub>2</sub> mixing ratios and  
437 provincial NO<sub>x</sub> emissions during the same period. From 1990 to 2002, f-NO<sub>3</sub><sup>-</sup> showed  
438 either no trend or a stable trend, which was consistent with the trend in the provincial  
439 NO<sub>x</sub> emissions, but inconsistent with the observed decreasing trend in NO<sub>2</sub> mixing ratio  
440 during this period. If looking at the full data record of c-NO<sub>3</sub><sup>-</sup> together (from 1990 to  
441 2012 in Victoria or 2015 in Vancouver), either no trend or a stable trend was identified  
442 in either city, regardless of using the full data record or just data after the year 2002.  
443 The absence of a clear decreasing trend in c-NO<sub>3</sub><sup>-</sup> concentration, despite significant  
444 NO<sub>x</sub> emissions, appears to be a common feature across Canadian urban environments.  
445 Unlike the other cities aforementioned where annual average concentrations of f-NO<sub>3</sub><sup>-</sup>  
446 were much higher than those of c-NO<sub>3</sub><sup>-</sup>, in Victoria, annual average concentrations of  
447 f-NO<sub>3</sub><sup>-</sup> and c-NO<sub>3</sub><sup>-</sup> were similar, oscillating around 0.23 ± 0.06 µg m<sup>-3</sup> (1990 to 2018)  
448 and 0.25 ± 0.05 µg m<sup>-3</sup> (1990 to 2012), respectively. In contrast, annual average  
449 concentrations of f-NO<sub>3</sub><sup>-</sup> (0.16 ± 0.05 µg m<sup>-3</sup> in 1990 - 2018) were significantly smaller  
450 than that of c-NO<sub>3</sub><sup>-</sup> (0.31 ± 0.05 µg m<sup>-3</sup> in 1990 - 2015) (*P*<0.01) in Vancouver, and the  
451 same conclusion can be generated if only using data in 1990-2015.

452

453 In Hamilton, no statistically significant trends were identified for f-NO<sub>3</sub><sup>-</sup> and c-NO<sub>3</sub><sup>-</sup>,  
454 whether considering the full time series or just the period post-2005. This is somewhat  
455 different than the cases in the other cities discussed above, suggesting potentially strong  
456 impact of local sources, besides the other main factors discussed above, considering  
457 that Hamilton is an industrial city with heavy density of industries. Annual average f-

458  $\text{NO}_3^-$  and  $\text{c-NO}_3^-$  in this city were  $0.88 \pm 0.35 \mu\text{g m}^{-3}$  and  $0.46 \pm 0.12 \mu\text{g m}^{-3}$ ,  
459 respectively, during the period of 1995 to 2019.

#### 460 **3.4 Key factors influencing annual average f- $\text{NO}_3^-$ and its trends in Edmonton**

461 To explore key factors influencing the annual average f- $\text{NO}_3^-$  and its trends in  
462 Edmonton, we selected data from two representative years (2010 and 2015) at site S-  
463 90132 for comparative analysis. The year 2010 was chosen because in this year  
464 abnormally high annual average f- $\text{NO}_3^-$  was observed compared to all the other years  
465 during the period of 2007-2019, suggesting possible impact by climate anomaly in this  
466 year. The year 2015 was chosen because in this year annual average f- $\text{NO}_3^-$  represents  
467 the median value of a five-year period of 2015-2019, likely reflecting the average  
468 climatic conditions, knowing that the annual average  $\text{NO}_2$  mixing ratio observed at a  
469 nearby site (S-90130) and the provincial total  $\text{NO}_x$  emissions were nearly constant  
470 during 2015-2019. From 2010 to 2015, the decrease in  $\text{NO}_2$  mixing ratios in Edmonton  
471 (11%) was consistent with the decline in Alberta's provincial  $\text{NO}_x$  emissions (10%). In  
472 contrast, the annual mean concentration of f- $\text{NO}_3^-$  decreased much more sharply (by  
473 58%), falling from  $2.1 \mu\text{g m}^{-3}$  in 2010 to  $0.89 \mu\text{g m}^{-3}$  in 2015.

474

475 Through the comparative analysis, seasonal variations of f- $\text{NO}_3^-$ , various single-factor  
476 effects on f- $\text{NO}_3^-$ , and the impact of climate anomalies on f- $\text{NO}_3^-$  were explored. As  
477 shown in Figures 3a and 3b, higher concentrations of f- $\text{NO}_3^-$  were predominantly  
478 observed during cold months, including January to March and November to December,  
479 in both 2010 and 2015. These higher concentrations during the five cold months  
480 contributed to 81% and 88% of the annual averages in 2015 and 2010, respectively.  
481 Thus, the annual trends in f- $\text{NO}_3^-$  were mainly determined by higher concentrations of  
482 f- $\text{NO}_3^-$  in cold months in Edmonton. Based on wind fields shown in Figures S1 and S2,  
483 air masses reaching to this site in the cold winter should come from the remote northern  
484 areas with low pollution levels due to the strong northwest wind, which should have  
485 lowered concentrations of f- $\text{NO}_3^-$  in the urban atmosphere. Thus, the high  
486 concentrations of f- $\text{NO}_3^-$  observed at this site should be caused by local accumulation

487 under stagnant weather conditions. Therefore, the emissions of f-NO<sub>3</sub><sup>-</sup>-contained  
488 aerosols related to mitigation measures, the precursors and formation pathways of f-  
489 NO<sub>3</sub><sup>-</sup>, and meteorological conditions during the winter period should be considered as  
490 key factors determining the annual average f-NO<sub>3</sub><sup>-</sup>.

491

492 We then correlated the 24-hr integrated daily concentrations of f-NO<sub>3</sub><sup>-</sup> with ambient T,  
493 wind speed (WS), RH, and HNO<sub>3gas</sub>\* to explore various single-factor effects on f-NO<sub>3</sub><sup>-</sup>  
494 (Figure 3). A demarcation line was observed at -3°C in 2010 and 0.5°C in 2015, with  
495 substantially lower f-NO<sub>3</sub><sup>-</sup> concentration at T on the right than left side of the line  
496 (Figures 3a and 3e). Lower ambient T favored the gas-aerosol partitioning of NH<sub>4</sub>NO<sub>3</sub>  
497 in PM<sub>2.5</sub> (Seinfeld and Pandis, 2016; Shah et al., 2018). However, lower ambient T also  
498 weakened photochemical reactions due to reduced amounts of intermediate volatility  
499 organic compounds or semi-volatile organic compounds in the gas phase (McDonald et  
500 al., 2018; Wernis et al., 2022). This reduction in photochemical activity subsequently  
501 lowered the concentration of HNO<sub>3gas</sub>\* to some extent, e.g., the concentrations of  
502 HNO<sub>3gas</sub>\* observed at T > 20°C increased by over a factor of four relative to those at T  
503 < -10°C in 2015 as shown in Figures 3e. The sources of f-NO<sub>3</sub><sup>-</sup> and its formation  
504 pathways during the winter period will be revisited in Section 3.5. The causes for the  
505 different T values of the demarcation line between 2010 and 2015 are not clear. The  
506 concentrations of f-NO<sub>3</sub><sup>-</sup> decreased with increasing WS due to the dispersion effect, and  
507 no elevated concentrations were observed once WS is stronger than 5 m/s (Figures 3b  
508 and 3f). The concentrations of f-NO<sub>3</sub><sup>-</sup> had little dependence on ambient RH (Figure 3c  
509 and 3g), e.g., the highest concentrations in both years occurred at RH of 70-80% instead  
510 of >80%. The lowest concentrations of f-NO<sub>3</sub><sup>-</sup> appearing at RH < 60% is because RH  
511 < 60% typically occurred at ambient T greater than 0°C in Edmonton. In addition, the  
512 relative importance of 15 major variables on f-NO<sub>3</sub><sup>-</sup> concentration was examined using  
513 a Random Forest model, as detailed in Text S2 of SI. The ambient T ranked as the  
514 dominant factor, followed by PM<sub>2.5</sub> mass concentration, NO<sub>2</sub> mixing ratio, boundary  
515 layer height, etc.

516

517 It should be noted that gas–particle equilibrium between  $\text{HNO}_3\text{--NH}_3$  and submicron  
518  $\text{NH}_4\text{NO}_3$  is unlikely to be achieved at temperatures below  $-10\text{ }^\circ\text{C}$ , given the relatively  
519 long equilibration timescales. Based on the results of characteristic timescales analysed  
520 by Wexler and Seinfeld (1990, 1992) and dynamically simulated by Meng and Seinfeld  
521 (1996), particles with diameters of approximately  $0.5\text{--}0.7\text{ }\mu\text{m}$  generally require hours  
522 to approach equilibrium – typically on the order of  $\sim 1\text{--}6\text{ h}$  with a more conservative  
523 upper bound of  $\sim 6\text{--}20\text{ h}$ . Under such low-temperature conditions, the assumption of  
524 instantaneous thermodynamic equilibrium becomes questionable; therefore,  
525 equilibrium thermodynamic modelling was not applied here. At even lower  
526 temperatures, the equilibration timescale would extend to tens of hours for highly  
527 viscous or glassy particles, as suggested by Li and Shiraiwa (2019).

528

529 Correlation analysis between simultaneously measured  $\text{f-NO}_3^-$  and  $\text{HNO}_{3\text{gas}}^*$  showed  
530 that  $\text{f-NO}_3^-$  concentrations higher than  $4\text{ }\mu\text{g m}^{-3}$  occurred when  $\text{HNO}_{3\text{gas}}^*$  concentrations  
531 were lower than  $0.4\text{ }\mu\text{g m}^{-3}$  in both years (Figures 3d and 3h). Thus, the high  $\text{f-NO}_3^-$   
532 concentrations were not likely caused from the secondary formation of  $\text{f-NO}_3^-$  from  
533  $\text{HNO}_{3\text{gas}}^*$  in ambient air, as further discussed in Section 3.5 below. Considering that the  
534 concentrations of  $\text{NH}_{3\text{gas}}$  (data not shown here) were generally more than one order of  
535 magnitude higher than those of  $\text{HNO}_{3\text{gas}}^*$ ,  $\text{NH}_{3\text{gas}}$  should not be the limiting factor for  
536  $\text{f-NO}_3^-$  formation, and was therefore excluded from further analysis below.

537

538 Climate anomaly can have significant impacts on air pollution (Andersson et al., 2007;  
539 Wetherbee and Mast, 2016; Yao and Zhang, 2020). One of the factors related to climate  
540 anomaly in winter Canadian urban atmospheres is AO (Burakowski et al., 2008;  
541 Higgins et al., 2002; Yao and Zhang, 2020). Other climate drivers, such as ENSO,  
542 Arctic sea-ice variability, and long-term warming, may influence  $\text{f-NO}_3^-$  during the  
543 warming season. However, their impact on the annual trend is likely negligible, as it is  
544 dominated by wintertime  $\text{f-NO}_3^-$ . As shown in Figures S1 and S2, the mean wind speed  
545 from January to March across Alberta decreased significantly in 2010 compared to the  
546 other years. The AO index during the winter period in 2010 was in the most negative

547 phase observed in the last four decades (Figure S1d). Typically, the belt of strong winds  
548 circulating around 55°N latitude weakens during such a phase, which allows colder  
549 Arctic air masses to penetrate further south into the mid-latitudes (Higgins et al., 2002).  
550 The substantial decrease in WS during the winter period of 2010 likely contributed to  
551 the higher annual average f-NO<sub>3</sub><sup>-</sup> in this year. It is noticed that the recorded ambient T  
552 in Edmonton in this winter was similar to the climatic mean value  
553 (<https://www.wunderground.com/about/data>), further supporting the hypothesis that it  
554 is the weakened WS caused by AO anomaly, rather than changes in T, that enhanced the  
555 accumulation of f-NO<sub>3</sub><sup>-</sup>.

556

557 To further examine the effects of the AO anomaly on f-NO<sub>3</sub><sup>-</sup> accumulation in 2010  
558 relative to that in 2015, we conducted the identical-percentile regression analysis  
559 between the two years (Figures 4c-e). With the intercept being forced to zero, similar  
560 to the approach commonly used in chemical experiments for establishing the standard  
561 curve (Yao et al., 2011), the slope of the regression equation was 2.74 if using all the  
562 data (0<sup>th</sup> to 100<sup>th</sup> percentiles), 1.56 if using the central 50% data (25<sup>th</sup> to 75<sup>th</sup> percentiles),  
563 and 1.41 if only using the lower 50% data (0<sup>th</sup> to 50<sup>th</sup> percentiles). The differences in f-  
564 NO<sub>3</sub><sup>-</sup> concentration between the two years were clearly enlarged when higher  
565 concentrations were included, due to the AO anomaly effect in the winter of 2010.  
566 Assuming a log-normal distribution of the data, the lower percentiles and higher  
567 percentiles data, i.e., 0<sup>th</sup> to 2.5<sup>th</sup> percentiles and 97.5<sup>th</sup> to 100<sup>th</sup> percentiles, are normally  
568 excluded from 95% confidence level. This is because these data points have lower  
569 probability densities and their corresponding values are more vulnerable to climate  
570 anomaly impact such as AO with negative and positive phases. The highest probability  
571 density should always occur at the 50<sup>th</sup> percentile, where the corresponding value  
572 should be least affected by AO. To minimize potential error from using a single value,  
573 we used the average values of the 47.5<sup>th</sup>-52.5<sup>th</sup> percentiles, which were 0.63 μg m<sup>-3</sup> in  
574 2010 and 0.45 μg m<sup>-3</sup> in 2015. The ratio of these two values (=1.4) was nearly identical  
575 to the slope of the regression equation using data from the 0<sup>th</sup> to 50<sup>th</sup> percentiles  
576 presented above. Thus, the annual average f-NO<sub>3</sub><sup>-</sup> in 2010 was recalculated by the

577 corresponding value in 2015 being multiplying by a factor of 1.4 in order to deduct the  
578 AO anomaly effect. The recalculated annual average f-NO<sub>3</sub><sup>-</sup> in 2010 would decrease  
579 from the original value of 2.1 µg m<sup>-3</sup> to 1.2 µg m<sup>-3</sup>. Interestingly, removing the AO  
580 effect in 2010 would only have a minor impact on the decadal trends from 2007 to 2019,  
581 e.g., the Sen's Slope only showed small changes: which was 0.063 µg m<sup>-3</sup> year<sup>-1</sup> using  
582 the original annual average values including the year 2010, 0.060 µg m<sup>-3</sup> year<sup>-1</sup> if  
583 excluding the year 2010, and 0.057 µg m<sup>-3</sup> year<sup>-1</sup> if replacing the year 2010 value with  
584 1.2 µg m<sup>-3</sup>.

585

586 Overall, the AO largely affected the annual average f-NO<sub>3</sub><sup>-</sup> in 2010. Nevertheless, such  
587 an impact only has marginal effects on the decadal trends of f-NO<sub>3</sub><sup>-</sup>, as the AO typically  
588 oscillates between negative and positive phases within 2-3 years (Figure S1d). The  
589 enhanced or weakened effects of AO in 2-3 years can be largely canceled out in  
590 extracting the decadal trend of f-NO<sub>3</sub><sup>-</sup>. The overall effect appeared to be too small to  
591 explain the above-mentioned disproportionate responses of the annual average f-NO<sub>3</sub><sup>-</sup>  
592 to the reduced NO<sub>x</sub> emissions, and more exploration on this issue is presented in  
593 Sections 3.5 and 3.6 below.

594

### 595 **3.5 Rethinking the role of primary emissions of NH<sub>4</sub>NO<sub>3</sub> during the cold season in** 596 **Canadian urban atmospheres**

597 From the analysis presented in the previous section we concluded that the high  
598 concentrations of f-NO<sub>3</sub><sup>-</sup> in the winter were mainly due to local accumulation under  
599 stagnant meteorological conditions, rather than long-range transport driven by north-  
600 westerly winds. This raised the fundamental question: what is the role of primary  
601 emissions in combustion plumes or secondary formation of NH<sub>4</sub>NO<sub>3</sub> in ambient air in  
602 contributing to f-NO<sub>3</sub><sup>-</sup> in Canadian urban atmospheres during the cold season? To  
603 answer this question, we proposed a hypothesis, i.e., whether HNO<sub>3</sub><sub>gas</sub>\* concentrations  
604 significantly increased under conditions with low f-NO<sub>3</sub><sup>-</sup> concentrations compared to  
605 cases with high f-NO<sub>3</sub><sup>-</sup> concentrations, and then examined the hypothesis below.

606 Theoretical analysis and implications of the hypothesis were provided in supplementary  
607 information (Text S4 of SI).

608

609 To examine the weaker hypothesis outlined above, we first divided the 2010  
610 observations into two temperature regimes:  $T < 0^{\circ}\text{C}$  and  $0^{\circ}\text{C} < T \leq 4^{\circ}\text{C}$ . Observations  
611 with  $T < 0^{\circ}\text{C}$  were further divided into two subsets based on  $\text{f-NO}_3^-$  concentrations,  
612 using the thresholds of  $> 4 \mu\text{g m}^{-3}$  and  $\leq 4 \mu\text{g m}^{-3}$ . These three groups were then  
613 compared, i.e., Group 1:  $T < 0^{\circ}\text{C}$  and  $\text{f-NO}_3^- > 4 \mu\text{g m}^{-3}$ , in which case there were 19  
614 samples with average  $\text{HNO}_{3\text{gas}}^*$  and  $\text{f-NO}_3^-$  concentrations being  $0.15 \pm 0.09 \mu\text{g m}^{-3}$  and  
615  $8.8 \pm 4.4 \mu\text{g m}^{-3}$ , respectively; Group 2:  $T < 0^{\circ}\text{C}$  and  $\text{f-NO}_3^- < 4 \mu\text{g m}^{-3}$ , in which case  
616 there were 26 samples with average  $\text{HNO}_{3\text{gas}}^*$  and  $\text{f-NO}_3^-$  concentrations being  $0.15 \pm$   
617  $0.12 \mu\text{g m}^{-3}$  and  $1.3 \pm 0.7 \mu\text{g m}^{-3}$ , respectively; and Group 3:  $0^{\circ}\text{C} < T \leq 4^{\circ}\text{C}$ , in which  
618 case there were 13 samples with average  $\text{HNO}_{3\text{gas}}^*$  and  $\text{f-NO}_3^-$  concentrations being  
619  $0.15 \pm 0.11 \mu\text{g m}^{-3}$  and  $1.3 \pm 1.7 \mu\text{g m}^{-3}$ , respectively. Apparently, the average  $\text{HNO}_{3\text{gas}}^*$   
620 concentrations did not differ between the three Groups ( $P < 0.01$ ); thus, the initial  
621 hypothesis has to be rejected. This suggests that the process of secondary formation of  
622  $\text{NH}_4\text{NO}_3$  from  $\text{HNO}_{3\text{gas}}^*$  was not the main contributor to the observed high  
623 concentrations of  $\text{f-NO}_3^-$ , leaving the process of primary emissions as the only major  
624 contributor. In addition, the markedly reduced  $\text{f-NO}_3^-$  concentrations at  $T > 0^{\circ}\text{C}$  were  
625 likely due to volatilization of a portion of primarily emitted  $\text{f-NO}_3^-$ .

626

627 To further test the robustness of the above analysis, we expanded the dataset to include  
628 measurements at  $T \leq 4^{\circ}$  from both 2010 and 2015, yielding a total of 108  $\text{f-NO}_3^-$   
629 samples (Group 1:  $n = 23$ ; Group 2:  $n = 54$ ; Group 3:  $n = 31$ ). The mean ( $\pm$  SD)  
630 concentrations of  $\text{f-NO}_3^-$  and  $\text{HNO}_{3\text{gas}}^*$  were  $8.7 \pm 4.1 \mu\text{g m}^{-3}$  and  $0.16 \pm 0.11 \mu\text{g m}^{-3}$   
631 for Group 1,  $1.4 \pm 0.95 \mu\text{g m}^{-3}$  and  $0.17 \pm 0.16 \mu\text{g m}^{-3}$  for Group 2, and  $0.9 \pm 1.1 \mu\text{g m}^{-3}$   
632  $^3$  and  $0.15 \pm 0.10 \mu\text{g m}^{-3}$  for Group 3, respectively. Even with the expanded dataset,  
633 mean  $\text{HNO}_{3\text{gas}}^*$  did not differ significantly among the three groups (Welch one-way  
634 ANOVA,  $P = 0.74$ ), despite the intentionally large contrast in  $\text{f-NO}_3^-$  imposed by the  
635 group definitions.

636

637 The above analysis results suggest that the trend of  $f\text{-NO}_3^-$  in Edmonton was likely  
638 governed by the primary emissions of  $f\text{-NO}_3^-$  aerosols, as well as the extents of their  
639 volatilization and dispersion during the cold season. The dependence of volatilization  
640 of  $f\text{-NO}_3^-$  on ambient T and dispersion on WS has been recently confirmed in  
641 observational and modeling studies (Huo et al., 2025; Peng et al., 2024; Shen et al.,  
642 2022). As mentioned in the Introduction, the primary emissions of  $f\text{-NO}_3^-$  likely have  
643 two major sources (or processes). The first source is also conventionally defined as  
644 condensable particulate emission and associated with the combustion of ( $\text{N}_2 + \text{O}_2$ ),  
645 which produces various oxidized nitrogen species, including  $\text{HNO}_{3\text{gas}}^*$ ,  $\text{NO}_x$ , etc.  
646 (USEPA, 2017). The amount of primary  $\text{NH}_4\text{NO}_3$  formed from  $\text{HNO}_{3\text{gas}}^*$  in cooling  
647 plumes theoretically depends on the combustion technology, the use of catalytic  
648 reduction systems employing  $\text{NH}_3$ , and the ambient T (Palash et al., 2013; Tayyeb Javed  
649 et al., 2007; Zhang et al., 2021), which may not be controlled by  $\text{NO}_x$  emission levels.  
650 In some reported cases, mitigation measures reduced  $\text{NO}_x$  emissions, but  
651 simultaneously increased primary emissions of  $f\text{-NO}_3^-$  (Feng et al., 2020; Palash et al.,  
652 2013; Tayyeb Javed et al., 2007; Yang et al., 2024; Zhao et al., 2020). As evidences  
653 presented in Sections 3.3, this phenomenon likely occurred across various Canadian  
654 urban atmospheres. In contrast, the second source in fresh cooling plumes is directly  
655 linked to  $\text{NO}_x$  emissions through the chemical conversion of  $\text{NO}_2$  in cooling plume  
656 droplets, although it is highly sensitive to the lifetime of these droplets (Shen et al.,  
657 2022; Wang et al., 2016; Wang et al., 2020). In addition, primary nitrate aerosols from  
658 traffic emissions were reportedly unimportant in urban atmospheres across Canada and  
659 U.S. (Chalbot et al., 2013; Jeong et al., 2020), leaving only one possibility that primary  
660 nitrate aerosols were mainly derived from stationary combustion sources.

661

662 Although secondary  $f\text{-NO}_3^-$  formation should always occur to some extent in ambient  
663 air, the relative contribution from this process to the total  $f\text{-NO}_3^-$  is very small during  
664 the periods with high  $f\text{-NO}_3^-$  concentrations. As shown in Text S3 of SI, the modeled  
665 maximum potential contribution from secondary formation can only account for a small

666 fraction of the observed  $f\text{-NO}_3^-$  (<15% in the baseline runs, and <45% even in the  
667 empirical-estimate runs known to have overpredictions in general). These results  
668 support the hypothesis presented above that primary  $f\text{-NO}_3^-$  was the dominant  
669 contributor to the high  $f\text{-NO}_3^-$  concentration in winter. Moreover, higher  $f\text{-NO}_3^-$   
670 concentrations were generally observed under low wind speeds ( $WS < 1\text{-}2 \text{ m s}^{-1}$ ). Given  
671 that the sampling site is about 17 km from the farthest urban edge, the transport time  
672 for both primary and secondary  $f\text{-NO}_3^-$  to reach the site was therefore estimated to be  
673 approximately 2–4 h. This timescale is far too short for substantial secondary formation  
674 of  $f\text{-NO}_3^-$  in such cold ambient air ( $T < -10 \text{ }^\circ\text{C}$ ), unless in-source processes dominated  
675 (Shen et al., 2022; USEPA, 2017; Zhang et al., 2023). Within this 2–4 h transport  
676 window, the amount of  $\text{HNO}_{3\text{gas}}$ \* dry deposition should also be minimum, especially  
677 under low-temperature conditions.

678

### 679 **3.6 Uncertainties affecting $f\text{-NO}_3^-$ trends in Edmonton**

680 Three categories of uncertainties that may affect the observed trends of  $f\text{-NO}_3^-$  in  
681 Edmonton were analyzed: (i) differences in observational results between the speciation  
682 sampler and the Dichotomous sampler, (ii) spatial inhomogeneity due to highly  
683 localized factors, and (iii) artifacts introduced by the sampling frequency (e.g., every  
684 third or sixth day), which may influence the calculation of annual averages. For  
685 category (i) uncertainty,  $\text{PM}_{2.5}$  mass concentrations measured by the two different  
686 instruments at site S-90132 in 2010 showed strong agreement for most samples, with  
687 occasional discrepancies at lower concentration levels (Figure S6). Specifically, when  
688 the regression intercept was forced to zero, the resulting equation was  $y = 1.02 * x$  ( $R^2 =$   
689  $0.94$ ), and the difference in annual average concentrations was less than 10% ( $10.3 \mu\text{g}$   
690  $\text{m}^{-3}$  from the Dichotomous sampler vs.  $11.1 \mu\text{g m}^{-3}$  from the speciation sampler).

691

692 For category (ii) uncertainty, Figure S7 compares real-time  $\text{PM}_{2.5}$  mass concentrations  
693 measured simultaneously at two sites 7 km apart (S-90132 and S-90130) from 2011 to  
694 2014. Other years were excluded due to significant data loss at one or both sites.

695 Regression slopes between the two sites (with intercepts forced to zero) are 0.86, 0.82,  
696 0.58, and 0.67, with corresponding differences in annual average concentrations of  
697 21%, 15%, 40%, and 39% in 2011, 2012, 2013, and 2014, respectively. The significant  
698 year-to-year differences between the two sites are unlikely caused by mitigation  
699 policies, climate variability, or changes in the atmospheric formation pathways of  
700 PM<sub>2.5</sub>, but rather by spatial inhomogeneity driven by highly localized factors that varied  
701 from year to year (Yeganeh et al., 2025). The influence of such localized effects appears  
702 to be substantial and may represent an important, yet often overlooked, contributor to  
703 the disproportionately large decreases in the annual average f-NO<sub>3</sub><sup>-</sup> relative to  
704 reductions in provincial total NO<sub>x</sub> emissions over decadal timescales. More broadly,  
705 pronounced intra-urban spatial heterogeneity has been documented for many ionic  
706 aerosol components (with sulfate generally exhibiting a more regional character),  
707 underscoring the importance of high-resolution urban monitoring for interpreting long-  
708 term trends. At the same time, compared with routine PM mass measurements,  
709 sustained long-term, high-resolution chemical speciation monitoring requires  
710 substantially greater investment in instrumentation, maintenance, and operational  
711 resources, making such measurements more challenging to maintain over multi-year  
712 periods. This practical limitation highlights the need to carefully consider site  
713 representativeness and spatial heterogeneity when interpreting long-term nitrate trends  
714 derived from fixed-site observations.

715

716 It is noted that while the annual average PM<sub>2.5</sub> mass concentrations were significantly  
717 higher at S-90130 than S-90132 ( $P < 0.01$ ) during 2010-2014, the opposite trend was  
718 observed for the annual average f-NO<sub>3</sub><sup>-</sup>, e.g., higher at S-90132 during 2007–2019  
719 compared to those at S-90130 during 1990–2005. The highest annual average f-NO<sub>3</sub><sup>-</sup>  
720 concentration at S-90130 appeared in 2000 and that at S-90132 appeared in 2010  
721 (Figure 1a). The mass fractions of f-NO<sub>3</sub><sup>-</sup> in PM<sub>2.5</sub> were  $0.050 \pm 0.065$  in 2000 and  $0.13$   
722  $\pm 0.13$  in 2010 (Figure S4), indicating that PM<sub>2.5</sub> at S-90132 contained more f-NO<sub>3</sub><sup>-</sup>  
723 aerosols during 2007-2019 than at S-90130 during 1990-2005, strongly supporting the  
724 hypothesis that mitigation measures reduced NO<sub>x</sub> emissions in Edmonton, while

725 simultaneously increased primary f-NO<sub>3</sub><sup>-</sup> emissions from the first source (see Section  
726 3.3) after 2005.

727

728 Concerning category (iii) uncertainty, no continuous measurements of f-NO<sub>3</sub><sup>-</sup> were  
729 available to assess its magnitude. We thus used continuous measurements of PM<sub>2.5</sub> data  
730 at S-90130 as a proxy for this evaluation. Given that the annual average PM<sub>2.5</sub> mass  
731 concentration in 2010 was approximately 50% larger than in 2011, the analysis was  
732 conducted using data from 2011 to 2020 instead of 2010 to 2020. Daily average PM<sub>2.5</sub>  
733 mass concentrations were first calculated for every day of the year. Then for each year,  
734 annual average PM<sub>2.5</sub> mass concentrations were calculated from daily average  
735 concentrations using (i) full dataset, (ii) one in every three days data (three subsets),  
736 and (iii) one in every six days data (six subsets). Thus, a total of 10 sets of annual  
737 average PM<sub>2.5</sub> data series was created for the period of 2011-2020, which was then used  
738 for decadal trend analysis. The trend derived from the full dataset showed a decreasing  
739 trend with a Sen's Slope of 0.43 μg m<sup>-3</sup> year<sup>-1</sup>. Consistent decreasing trends were also  
740 obtained from using the one in every three days subset data series, with Sen's Slope  
741 values of 0.46, 0.46, and 0.42 μg m<sup>-3</sup> year<sup>-1</sup>, respectively, indicating an error of less than  
742 8%. When using the one in every six days subset data series, five out of six data subsets  
743 also showed a decreasing trend, with Sen's Slope values of 0.47, 0.50, 0.45, 0.45, and  
744 0.44 μg m<sup>-3</sup> year<sup>-1</sup>, respectively, indicating an error of less than 10% in most cases.  
745 However, one subset data series showed a probable decreasing trend, with a Sen's Slope  
746 of 0.38 μg m<sup>-3</sup> year<sup>-1</sup>.

747

748 Using the same approach described above, we also compared the decadal trends  
749 obtained from using one in every three days data, which are readily available, with those  
750 from using one in every six days data, which are arbitrarily split from the former data  
751 set into two subsets. One of the two subsets for f-NO<sub>3</sub><sup>-</sup> showed a decreasing trend with  
752 a Sen's Slope of 0.055 μg m<sup>-3</sup> year<sup>-1</sup>, which is close to the original value of 0.063 μg m<sup>-3</sup>  
753 year<sup>-1</sup>; however, the other subset exhibited a stable trend. For f-SO<sub>4</sub><sup>2-</sup>, both subsets  
754 showed decreasing trends, with Sen's Slope values of 0.033 and 0.018 μg m<sup>-3</sup> year<sup>-1</sup>,

755 respectively, although deviating to some extent from the original estimate of  $0.022 \mu\text{g}$   
756  $\text{m}^{-3} \text{year}^{-1}$ . For  $\text{f-NH}_4^+$ , both subsets showed stable trends, consistent with the results  
757 derived from the original dataset. Overall, using one in every three or six days data can  
758 generate decadal trends with reasonable accuracy, although the obtained trends need to  
759 be interpreted carefully when the trends are not significant or the changing rates are  
760 very small.

761

762 In the literature (Text S1 of SI), changes in atmospheric  $\text{NH}_3$  and  $\text{f-SO}_4^{2-}$  have been  
763 reported to influence long-term trends in  $\text{f-NO}_3^-$  to some extent. However, evidence of  
764 increasing atmospheric  $\text{NH}_3$  in Canada, together with reduced  $\text{NH}_3$  consumption for  
765 neutralizing the two major inorganic acids, suggests that  $\text{NH}_3$  is generally abundant and  
766 unlikely to be the limiting factor for  $\text{f-NO}_3^-$  formation (Yao and Zhang, 2019).  
767 Consistent with this interpretation, large  $\text{f-NO}_3^-/\text{f-SO}_4^{2-}$  mass ratios are frequently  
768 observed in high- $\text{f-NO}_3^-$  samples during the cold season across Canada. For example,  
769 in Edmonton in 2010, samples with  $\text{f-NO}_3^- > 4 \mu\text{g m}^{-3}$  exhibited  $\text{f-NO}_3^-/\text{f-SO}_4^{2-}$  mass  
770 ratios ranging from 1.5 to 12, with a median of 5.5. These results indicate that the  
771 elevated  $\text{f-NO}_3^-$  concentrations overwhelmingly dominated its long-term trend. In such  
772 cases, the slight decrease in  $\text{f-SO}_4^{2-}$  may exert only a minor influence on the trend in  $\text{f-}$   
773  $\text{NO}_3^-$ . Nevertheless, these complex interactions warrant further investigation using  
774 three-dimensional (3-D) air quality modelling; however, such efforts remain  
775 challenging, as illustrated below.

776

777 Existing studies using 3-D chemical transport models (CTMs) simulating particulate  
778  $\text{NO}_3^-$  over North America are summarized in Text S5 of SI. Several key points can be  
779 generated from these studies. (1) CTMs are widely applied and can often reproduce  
780 broad spatial patterns and major controlling processes of particulate  $\text{NO}_3^-$  over the  
781 United States and Canada; however, they frequently exhibit systematic biases in  
782 magnitude, long-term trends, and sensitivities to emission controls, with a substantial  
783 risk of error compensation (ECCC, 2016; Kim et al., 2014, 2023; Luo et al., 2019;  
784 Pappin et al., 2024; Pun et al., 2009; Russell et al., 2019; Semeniuk et al., 2025; Shah

785 et al., 2018; Smyth et al., 2009; Walker et al., 2012). (2) The standard GEOS-Chem  
786 v12.0.0 simulation substantially overestimated surface  $\text{PM}_{2.5} \text{NO}_3^-$  over the U.S. ( $1.89$   
787  $\mu\text{g m}^{-3}$  vs.  $0.70 \mu\text{g m}^{-3}$ ), with pronounced spatial heterogeneity: outside California, the  
788 normalized mean bias reached +176%, whereas California exhibited an opposite bias  
789 of -62%, implying region-dependent dominant error sources (e.g., meteorology,  
790 emissions, and/or thermodynamics) (Luo et al., 2019; Walker et al., 2012). (3)  
791 simulated particulate  $\text{NO}_3^-$  often responds to  $\text{NO}_x$  controls in a strongly non-linear, and  
792 sometimes counterintuitive manner, posing a persistent “acidity–partitioning”  
793 challenge for trend attribution. For instance, in the northeastern United States,  
794 observations show that  $\text{PM}_{10}$  nitrate increased by 95% (urban) and 57% (rural) from  
795 2005 to 2015 despite declining  $\text{NO}_x$  emissions, and this behavior was attributed to  
796 changes in aerosol acidity and gas–particle partitioning feedbacks that can offset the  
797 expected effect of precursor reductions (Kim et al., 2023). Finally, condensable  
798 particulate nitrate, as defined in US EPA Method 202 (US EPA, 2017), as well as its  
799 enhanced fraction under sub-freezing conditions, is generally not represented in current  
800 emission inventories. Given its potential importance, as suggested by our analysis  
801 presented above, incorporating temperature-dependent condensable nitrate into  
802 emission inventories is likely necessary to improve the representation and prediction of  
803 f- $\text{NO}_3^-$  in 3-D air quality modelling.

804

#### 805 **4 Findings and implications**

806 The in-depth analysis results presented in this study demonstrate that the dynamics of  
807 particulate nitrate in Canadian urban atmospheres are governed by complex interactions  
808 among emission reductions, primary sources, and cold-climate meteorology. Three key  
809 insights emerge:

810

811 (i) Non-linear responses of f- $\text{NO}_3^-$  to  $\text{NO}_x$  emission reductions in all the cities: Early  
812 phase implementation of  $\text{NO}_x$  control measures paradoxically increased f- $\text{NO}_3^-$  during

813 1998–2007, likely due to altered combustion plume chemistry favoring rapid f-NO<sub>3</sub><sup>-</sup>  
814 formation in cold-climate conditions. Significant declines in f-NO<sub>3</sub><sup>-</sup> (e.g., 60% in  
815 Edmonton) outpaced NO<sub>x</sub> reductions in the most recent decade, driven by diminishing  
816 primary emissions, highly localized factors, and AO induced dispersion effects.

817

818 (ii) Decoupled c-NO<sub>3</sub><sup>-</sup> and NO<sub>x</sub> reductions in all the cities except Edmonton: c-NO<sub>3</sub><sup>-</sup>  
819 remained stable or increased slightly while NO<sub>x</sub> emissions were reduced. c-NO<sub>3</sub><sup>-</sup> trends  
820 were likely controlled by the abundance of alkali aerosols, highlighting the limited  
821 efficacy of NO<sub>x</sub>-focused policies for controlling c-NO<sub>3</sub><sup>-</sup>.

822

823 (iii) Critical role of primary f-NO<sub>3</sub><sup>-</sup> emissions in winter in all the cities: Over 80% of  
824 the annual f-NO<sub>3</sub><sup>-</sup> burden was originated from cold-season primary emissions, with  
825 minimal contribution from secondary formation process, emphasizing the need for  
826 season-specific mitigation strategies. However, confirmation of this role requires three-  
827 dimensional air quality modeling with updated emission inventories that explicitly  
828 incorporate condensable particulate matter under subzero ambient temperatures.

829

830 Collectively, these findings call for a paradigm shift in air quality management.  
831 Effective mitigation strategies must explicitly address primary particulate nitrate  
832 sources, incorporate gas–particle partitioning dynamics under cold-climate conditions,  
833 and account for interactions with alkali-containing aerosols. Policy frameworks should  
834 further prioritize enhanced real-time measurements of PM<sub>2.5</sub> chemical composition to  
835 better resolve localized and seasonal variability, particularly in regions experiencing  
836 prolonged winter conditions. In parallel, coordinated unmanned aerial vehicle and  
837 ground-based observations of CPM under contrasting temperature and atmospheric  
838 dispersion regimes are essential to provide direct observational evidence of its role and  
839 contributions.

840

841 **Acknowledgement.** QF and XY are supported by the Natural Science Foundation of  
842 China (grant no. 41776086). We greatly appreciate all the personnel of the NAPS  
843 Partners who operate the sites across Canada and collect the field samples, and the  
844 staff of the Analysis and Air Quality Section in Ottawa for the laboratory chemical  
845 analyses and QA/QC of the data used in the present study. NPRI/APEI groups are also  
846 acknowledged for their efforts in generating emissions data across Canada.

847 *Data availability.* The access of the data used in this study is described in Section 2  
848 above.

849 *Author Contributions.* QF, XY and LZ designed the research, conducted the data  
850 analysis and wrote the manuscript.

851 *Competing interests.* One of the coauthors is a member of the editorial board of ACP.

852

## 853 **References**

- 854 Aas, W., Mortier, A., and Bowersox, V. et al.: Global and regional trends of atmospheric sulfur, *Sci. Rep.*,  
855 9, 953, 10.1038/s41598-018-37304-0, 2019.
- 856 Andersson, C., Langner, J., and Bergström, R.: Interannual variation and trends in air pollution over  
857 Europe due to climate variability during 1958–2001 simulated with a regional CTM coupled to the  
858 ERA40 reanalysis, *Tellus Ser. B-Chem. Phys. Meteorol.*, 59, 77-98, 10.1111/j.1600-  
859 0889.2006.00196.x, 2007.
- 860 Balamurugan, V., Chen, J., and Qu, Z. et al.: Secondary PM<sub>2.5</sub> decreases significantly less than NO<sub>2</sub>  
861 emission reductions during COVID lockdown in Germany, *Atmos. Chem. Phys.*, 22, 7105-7129,  
862 10.5194/acp-22-7105-2022, 2022.
- 863 Bari, M. A., and Kindzierski, W. B.: Fine particulate matter (PM<sub>2.5</sub>) in Edmonton, Canada: source  
864 apportionment and potential risk for human health, *Environ. Pollut.*, 218, 219-229,  
865 10.1016/j.envpol.2016.06.014, 2016a.
- 866 Bari, M. A., and Kindzierski, W. B.: Eight-year (2007–2014) trends in ambient fine particulate matter  
867 (PM<sub>2.5</sub>) and its chemical components in the capital region of Alberta, Canada, *Environ. Int.*, 91, 122-  
868 132, 10.1016/j.envint.2016.02.033, 2016b.
- 869 Bell, M. L., Dominici, F., and Ebisu, K. et al.: Spatial and temporal variation in PM<sub>2.5</sub> chemical  
870 composition in the United States for health effects studies, *Environ. Health. Perspect.*, 115, 989-995,  
871 10.1289/ehp.9621, 2007.
- 872 Bose, S., Rosa, M. J., and Mathilda Chiu, Y. et al.: Prenatal nitrate air pollution exposure and reduced  
873 child lung function: timing and fetal sex effects, *Environ. Res.*, 167, 591-597,  
874 <https://doi.org/10.1016/j.envres.2018.08.019>, 2018.
- 875 Burakowski, E. A., Wake, C. P., Braswell, B., and Brown, D. P.: Trends in wintertime climate in the  
876 northeastern united states: 1965–2005, *J. Geophys. Res. Atmos.*, 113, D20114,

877 10.1029/2008JD009870, 2008.

878 Canada Electricity Advisory Council: Powering Canada: A blueprint for success., 2024.

879 Chalbot, M. C., McElroy, B., and Kavouras, I. G.: Sources, trends and regional impacts of fine particulate  
880 matter in Southern Mississippi Valley: significance of emissions from sources in the Gulf of Mexico  
881 coast, *Atmos. Chem. Phys.*, 13, 3721-3732, 10.5194/acp-13-3721-2013, 2013.

882 Chan, Y., Evans, M. J., and He, P. et al.: Heterogeneous nitrate production mechanisms in intense haze  
883 events in the North China Plain, *J. Geophys. Res.-Atmos.*, 126, e2021JD034688,  
884 10.1029/2021JD034688, 2021.

885 Chen, G., Fan, X., and Yu, S. et al.: HOCl formation driven by photochemical processes enhanced  
886 atmospheric oxidation capacity in a coastal atmosphere, *Environ. Sci. Technol.*, 59, 5164-5171,  
887 10.1021/acs.est.5c01363, 2025.

888 Cheng, B., Alapaty, K., and Arunachalam, S.: Spatiotemporal trends in PM<sub>2.5</sub> chemical composition in  
889 the conterminous U.S. During 2006–2020, *Atmos. Environ.*, 316, 120188,  
890 10.1016/j.atmosenv.2023.120188, 2024.

891 Cheng, I., and Zhang, L.: Long-term air concentrations, wet deposition, and scavenging ratios of  
892 inorganic ions, HNO<sub>3</sub>, and SO<sub>2</sub> and assessment of aerosol and precipitation acidity at Canadian rural  
893 locations, *Atmos. Chem. Phys.*, 17, 4711-4730, 10.5194/acp-17-4711-2017, 2017.

894 Dabek-Zlotorzynska, E., Celo, V., and Ding, L. et al.: Characteristics and sources of PM<sub>2.5</sub> and reactive  
895 gases near roadways in two metropolitan areas in Canada, *Atmos. Environ.*, 218, 116980,  
896 10.1016/j.atmosenv.2019.116980, 2019.

897 Dabek-Zlotorzynska, E., Dann, T. F., and Kalyani Martinelango, P. et al.: Canadian national air pollution  
898 surveillance (NAPS) PM<sub>2.5</sub> speciation program: methodology and PM<sub>2.5</sub> chemical composition for the  
899 years 2003–2008, *Atmos. Environ.*, 45, 673-686, 10.1016/j.atmosenv.2010.10.024, 2011.

900 Dang, R., Jacob, D. J., and Zhai, S. et al.: A satellite-based indicator for diagnosing particulate nitrate  
901 sensitivity to precursor emissions: application to East Asia, Europe, and North America, *Environ. Sci.*  
902 *Technol.*, 58, 20101-20113, 10.1021/acs.est.4c08082, 2024.

903 Drugé, T., Nabat, P., Mallet, M., and Somot, S.: Model simulation of ammonium and nitrate aerosols  
904 distribution in the euro-mediterranean region and their radiative and climatic effects over 1979–2016,  
905 *Atmos. Chem. Phys.*, 19, 3707-3731, 10.5194/acp-19-3707-2019, 2019.

906 Duce, R. A., LaRoche, J., and Altieri, K. et al.: Impacts of atmospheric anthropogenic nitrogen on the  
907 open ocean, *Science*, 320, 893-897, 10.1126/science.1150369, 2008.

908 ECCC: Canada – United States transboundary particulate matter science assessment 2013, 2016.

909 ECCC: Environment and climate change Canada: Canadian environmental sustainability indicators: air  
910 pollutant emissions, available at: [https://www.canada.ca/en/environment-climate-  
911 change/services/environmental-indicators/air-pollutant-emissions.html](https://www.canada.ca/en/environment-climate-change/services/environmental-indicators/air-pollutant-emissions.html), last access: 13 November  
912 2021., in, edited, 2021.

913 Edgerton, E. S., Hsu, Y., and White, E. M. et al.: Ambient concentrations and total deposition of inorganic  
914 sulfur, inorganic nitrogen and base cations in the Athabasca oil sands region, *Sci. Total Environ.*, 706,  
915 134864, 10.1016/j.scitotenv.2019.134864, 2020.

916 Fan, M., Zhang, Y., and Lin, Y. et al.: Changes of emission sources to nitrate aerosols in Beijing after the  
917 clean air actions: evidence from dual isotope compositions, *J. Geophys. Res.-Atmos.*, 125,  
918 e2019JD031998, 10.1029/2019JD031998, 2020.

919 Feng, J., Chan, E., and Vet, R.: Air quality in the eastern united states and Eastern Canada for 1990–

920 2015: 25 years of change in response to emission reductions of SO<sub>2</sub> and NO<sub>x</sub> in the region, *Atmos.*  
921 *Chem. Phys.*, 20, 3107-3134, 10.5194/acp-20-3107-2020, 2020.

922 Font, A., de Brito, J. F., and Riffault, V. et al.: Long-term measurements of aerosol composition at rural  
923 background sites in France: sources, seasonality and mass closure of PM<sub>2.5</sub>, *Atmos. Environ.*, 334,  
924 120724, 10.1016/j.atmosenv.2024.120724, 2024.

925 Gen, M., Liang, Z., and Zhang, R. et al.: Particulate nitrate photolysis in the atmosphere, *Environmental*  
926 *Science: Atmospheres*, 2, 111-127, 10.1039/d1ea00087j, 2022.

927 Guo, T., Li, K., and Zhu, Y. et al.: Concentration and size distribution of particulate oxalate in marine  
928 and coastal atmospheres – implication for the increased importance of oxalate in nanometer  
929 atmospheric particles, *Atmos. Environ.*, 142, 19-31, 10.1016/j.atmosenv.2016.07.026, 2016.

930 Hand, J. L., Prenni, A. J., and Schichtel, B. A.: Trends in seasonal mean speciated aerosol composition  
931 in remote areas of the United States from 2000 through 2021, *J. Geophys. Res.-Atmos.*, 129,  
932 e2023JD039902, 10.1029/2023JD039902, 2024.

933 Harrison, R. M., Beddows, D. C. S., Tong, C., and Damayanti, S.: Non-linearity of secondary pollutant  
934 formation estimated from emissions data and measured precursor-secondary pollutant relationships,  
935 *npj Clim. Atmos. Sci.*, 5, 71, 10.1038/s41612-022-00297-9, 2022.

936 He, K., Yang, F., and Ma, Y. et al.: The characteristics of PM<sub>2.5</sub> in Beijing, China, *Atmos. Environ.*, 35,  
937 4959-4970, 10.1016/S1352-2310(01)00301-6, 2001.

938 Higgins, R. W., Leetmaa, A., and Kousky, V. E.: Relationships between climate variability and winter  
939 temperature extremes in the United States, *J. Clim.*, 15, 1555-1572, 10.1175/1520-  
940 0442(2002)015<1555:RBCVAW>2.0.CO;2, 2002.

941 Höpfner, M., Ungermann, J., and Borrmann, S. et al.: Ammonium nitrate particles formed in upper  
942 troposphere from ground ammonia sources during Asian monsoons, *Nat. Geosci.*, 12, 608-612,  
943 10.1038/s41561-019-0385-8, 2019.

944 Huo, H., Gao, Y., and Sun, L. et al.: Investigating dual character of atmospheric ammonia on particulate  
945 NH<sub>4</sub>NO<sub>3</sub>: reducing evaporation versus promoting formation, *Atmosphere*, 16, 685,  
946 10.3390/atmos16060685, 2025.

947 Iizuka, Y., Matsumoto, M., and Kawakami, K. et al.: Acidity-driven gas-particle partitioning of nitrate  
948 regulates its transport to arctic through the industrial era, *Nat. Commun.*, 16, 4272, 10.1038/s41467-  
949 025-59208-0, 2025.

950 Jeong, C. H., McGuire, M. L., and Herod, D. et al.: Receptor model based identification of PM<sub>2.5</sub> sources  
951 in canadian cities, *Atmos. Pollut. Res.*, 2, 158-171, 10.5094/APR.2011.021, 2011.

952 Jeong, C., Traub, A., and Huang, A. et al.: Long-term analysis of PM<sub>2.5</sub> from 2004 to 2017 in Toronto:  
953 composition, sources, and oxidative potential, *Environ. Pollut.*, 263, 114652,  
954 10.1016/j.envpol.2020.114652, 2020.

955 Jonson, J. E., Fagerli, H., Scheuschner, T., and Tsyro, S.: Modelling changes in secondary inorganic  
956 aerosol formation and nitrogen deposition in Europe from 2005 to 2030, *Atmos. Chem. Phys.*, 22,  
957 1311-1331, 10.5194/acp-22-1311-2022, 2022.

958 Kim, H., Walters, W. W., Kysela, L., and Hastings, M. G.: Long-term trends in inorganic aerosol  
959 chemical composition and chemistry at an urban and rural site in the Northeastern US, *Sci. Total*  
960 *Environ.*, 904, 166848, 10.1016/j.scitotenv.2023.166848, 2023.

961 Kim, Y. J., Spak, S. N., and Carmichael, G. R. et al.: Modeled aerosol nitrate formation pathways during  
962 wintertime in the Great Lakes region of North America, *J. Geophys. Res.-Atmos.*, 119, 12, 412-420,  
963 445, 10.1002/2014JD022320, 2014.

964 Li, Y., and Shiraiwa, M.: Timescales of secondary organic aerosols to reach equilibrium at various  
965 temperatures and relative humidities, *Atmos. Chem. Phys.*, 19, 5959-5971, 10.5194/acp-19-5959-  
966 2019, 2019.

967 Lin, Y., Zhang, L., and Fan, Q. et al.: Decoupling impacts of weather conditions on interannual variations  
968 in concentrations of criteria air pollutants in South China -- constraining analysis uncertainties by  
969 using multiple analysis tools, *Atmos. Chem. Phys.*, 22, 16073-16090, 10.5194/acp-22-16073-2022,  
970 2022.

971 Luo, G., Yu, F., and Schwab, J.: Revised treatment of wet scavenging processes dramatically improves  
972 GEOS-chem 12.0.0 simulations of surface nitric acid, nitrate, and ammonium over the United States,  
973 *Geosci. Model Dev.*, 12, 3439-3447, 10.5194/gmd-12-3439-2019, 2019.

974 Man, H., Zhu, Y., and Ji, F. et al.: Comparison of daytime and nighttime new particle growth at the  
975 HKUST supersite in Hong Kong, *Environ. Sci. Technol.*, 49, 7170-7178, 10.1021/acs.est.5b02143,  
976 2015.

977 McDonald, B. C., de Gouw, J. A., and Gilman, J. B. et al.: Volatile chemical products emerging as largest  
978 petrochemical source of urban organic emissions, *Science*, 359, 760-764, 10.1126/science.aaq0524,  
979 2018.

980 Meng, Z., and Seinfeld, J. H.: Time scales to achieve atmospheric gas-aerosol equilibrium for volatile  
981 species, *Atmos. Environ.*, 30, 2889-2900, [https://doi.org/10.1016/1352-2310\(95\)00493-9](https://doi.org/10.1016/1352-2310(95)00493-9), 1996.

982 Palash, S. M., Masjuki, H. H., and Kalam, M. A. et al.: State of the art of NO<sub>x</sub> mitigation technologies  
983 and their effect on the performance and emission characteristics of biodiesel-fueled compression  
984 ignition engines, *Energy Conv. Manag.*, 76, 400-420, 10.1016/j.enconman.2013.07.059, 2013.

985 Pappin, A. J., Charman, N., and Egyed, M. et al.: Attribution of fine particulate matter and ozone health  
986 impacts in Canada to domestic and US emission sources, *Sci. Total Environ.*, 909, 168529,  
987 10.1016/j.scitotenv.2023.168529, 2024.

988 Park, R. J., Jacob, D. J., and Field, B. D. et al.: Natural and transboundary pollution influences on sulfate-  
989 nitrate-ammonium aerosols in the United States: implications for policy, *J. Geophys. Res. Atmos.*,  
990 109, 10.1029/2003JD004473, 2004.

991 Peng, W., Zhu, B., and Kang, H. et al.: Inconsistent 3-d structures and sources of sulfate ammonium and  
992 nitrate ammonium aerosols during cold front episodes, *J. Geophys. Res.-Atmos.*, 129,  
993 e2023JD039958, 10.1029/2023JD039958, 2024.

994 Peng, X., Wang, T., and Wang, W. et al.: Photodissociation of particulate nitrate as a source of daytime  
995 tropospheric  $\text{Cl}_2$ , *Nat. Commun.*, 13, 939, 10.1038/s41467-022-28383-9, 2022.

996 Pullokaran, D., Bhardwaj, A., and Haswani, D. et al.: Spatio-temporal trends of the relationships between  
997 surface  $\text{PM}_{2.5}$  and its chemical constituents across three COALESCE network locations in India: a  
998 mass closure investigation, *J. Geophys. Res.-Atmos.*, 129, e2023JD039855, 10.1029/2023JD039855,  
999 2024.

1000 Pun, B. K., Balmori, R. T. F., and Seigneur, C.: Modeling wintertime particulate matter formation in  
1001 central California, *Atmos. Environ.*, 43, 402-409, 10.1016/j.atmosenv.2008.08.040, 2009.

1002 Qi, J., Liu, X., and Yao, X. et al.: The concentration, source and deposition flux of ammonium and nitrate  
1003 in atmospheric particles during dust events at a coastal site in Northern China, *Atmos. Chem. Phys.*,  
1004 18, 571-586, 10.5194/acp-18-571-2018, 2018.

1005 Russell, M., Hakami, A., and Makar, P. A. et al.: An evaluation of the efficacy of very high resolution  
1006 air-quality modelling over the Athabasca oil sands region, Alberta, Canada, *Atmos. Chem. Phys.*, 19,  
1007 4393-4417, 10.5194/acp-19-4393-2019, 2019.

1008 Seinfeld, J. H., and Pandis, S. N.: *Atmospheric chemistry and physics: from air pollution to climate  
1009 change*. Third edition. Hoboken, new jersey: John Wiley & Sons, inc., in, edited, 2016.

1010 Semeniuk, K., Dastoor, A., and Lupu, A.: Implementation of the MOSAIC aerosol module (v1.0) in the  
1011 Canadian air quality model GEM-MACH (v3.1), *Geosci. Model Dev.*, 18, 6479-6515, 10.5194/gmd-  
1012 18-6479-2025, 2025.

1013 Shah, V., Jaeglé, L., and Thornton, J. A. et al.: Chemical feedbacks weaken the wintertime response of  
1014 particulate sulfate and nitrate to emissions reductions over the eastern united states, *Proc. Natl. Acad.  
1015 Sci.*, 115, 8110-8115, 10.1073/pnas.1803295115, 2018.

1016 Shen, Y., Meng, H., and Yao, X. et al.: Does ambient secondary conversion or the prolonged fast  
1017 conversion in combustion plumes cause severe PM<sub>2.5</sub> air pollution in China? *Atmosphere*, 13, 673,  
1018 10.3390/atmos13050673, 2022.

1019 Sickles II, J. E., and Shadwick, D. S.: Air quality and atmospheric deposition in the eastern US: 20 years  
1020 of change, *Atmos. Chem. Phys.*, 15, 173-197, 10.5194/acp-15-173-2015, 2015.

1021 Smyth, S. C., Jiang, W., and Roth, H. et al.: A comparative performance evaluation of the AURAMS and  
1022 CMAQ air-quality modelling systems, *Atmos. Environ.*, 43, 1059-1070,  
1023 10.1016/j.atmosenv.2008.11.027, 2009.

1024 Squizzato, S., Masiol, M., Rich, D. Q., and Hopke, P. K.: PM<sub>2.5</sub> and gaseous pollutants in New York  
1025 state during 2005–2016: spatial variability, temporal trends, and economic influences, *Atmos.  
1026 Environ.*, 183, 209-224, 10.1016/j.atmosenv.2018.03.045, 2018.

1027 Statistics Canada: New motor vehicle registrations, fourth quarter 2023, *The Daily*, released 12 March  
1028 2024, available at: <https://www150.statcan.gc.ca/n1/daily-quotidien/240312/dq240312c-eng.htm>  
1029 (last access: 24 February 2026), 2024.

1030 Sun, P., Wang, J., and Liu, Y. et al.: Enhanced particulate nitrate formation in residual layer exacerbates  
1031 near-surface pollution: insights from tethered airship and long-term ground measurements, *J. Geophys.  
1032 Res.-Atmos.*, 130, e2024JD042672, 10.1029/2024JD042672, 2025.

1033 Sun, W., Shao, M., and Granier, C. et al.: Long-term trends of anthropogenic so, NO, CO, and NMVOCs  
1034 emissions in China, *Earth's Future*, 6, 1112-1133, 10.1029/2018EF000822, 2018.

1035 Tang, Y. S., Braban, C. F., and Dragosits, U. et al.: Acid gases and aerosol measurements in the UK  
1036 (1999--2015): regional distributions and trends, *Atmos. Chem. Phys.*, 18, 16293-16324, 10.5194/acp-  
1037 18-16293-2018, 2018.

1038 Tayyeb Javed, M., Irfan, N., and Gibbs, B. M.: Control of combustion-generated nitrogen oxides by

1039 selective non-catalytic reduction, *J. Environ. Manage.*, 83, 251-289, 10.1016/j.jenvman.2006.03.006,  
1040 2007.

1041 Thunis, P., Clappier, A., and Beekmann, M. et al.: Non-linear response of PM<sub>2.5</sub> to changes in NO<sub>x</sub> and  
1042 NH<sub>3</sub> emissions in the Po basin (Italy): consequences for air quality plans, *Atmos. Chem. Phys.*, 21,  
1043 9309-9327, 10.5194/acp-21-9309-2021, 2021.

1044 USEPA: Method 202—dry impinger method for determining condensable particulate emissions from  
1045 stationary sources, Emission Measurement Center, Research Triangle Park, NC, USA, 2017.

1046 Velazquez-Garcia, A., Crumeyrolle, S., and de Brito, J. F. et al.: Deriving composition-dependent aerosol  
1047 absorption, scattering and extinction mass efficiencies from multi-annual high time resolution  
1048 observations in northern France, *Atmos. Environ.*, 298, 119613, 10.1016/j.atmosenv.2023.119613,  
1049 2023.

1050 Walker, J. M., Philip, S., Martin, R. V., and Seinfeld, J. H.: Simulation of nitrate, sulfate, and ammonium  
1051 aerosols over the United States, *Atmos. Chem. Phys.*, 12, 11213-11227, 10.5194/acp-12-11213-2012,  
1052 2012.

1053 Wang, G., Zhang, R., and Gomez, M. E. et al.: Persistent sulfate formation from London fog to Chinese  
1054 haze, *Proc. Natl. Acad. Sci.*, 113, 13630-13635, 10.1073/pnas.1616540113, 2016.

1055 Wang, H., Wang, H., and Lu, X. et al.: Increased night-time oxidation over China despite widespread  
1056 decrease across the globe, *Nat. Geosci.*, 16, 217-223, 10.1038/s41561-022-01122-x, 2023.

1057 Wang, H., Zhang, L., and Cheng, I. et al.: Spatiotemporal trends of PM<sub>2.5</sub> and its major chemical  
1058 components at urban sites in Canada, *J. Environ. Sci.*, 103, 1-11, 10.1016/j.jes.2020.09.035, 2021.

1059 Wang, M., Kong, W., and Marten, R. et al.: Rapid growth of new atmospheric particles by nitric acid and  
1060 ammonia condensation, *Nature*, 581, 184-189, 10.1038/s41586-020-2270-4, 2020.

1061 Wang, M., Xiao, M., and Bertozzi, B. et al.: Synergistic HNO<sub>3</sub>-H<sub>2</sub>SO<sub>4</sub>-NH<sub>3</sub> upper tropospheric particle  
1062 formation, *Nature*, 605, 483-489, 10.1038/s41586-022-04605-4, 2022.

1063 Ward, R. X., Baliaka, H. D., and Schulze, B. C. et al.: Poorly quantified trends in ammonium nitrate  
1064 remain critical to understand future urban aerosol control strategies, *Sci. Adv.*, 11, eadt8957,  
1065 10.1126/sciadv.adt8957, 2025.

1066 Wernis, R. A., Kreisberg, N. M., and Weber, R. J. et al.: Source apportionment of VOCs, IVOCs and  
1067 SVOCs by positive matrix factorization in suburban Livermore, California, *Atmos. Chem. Phys.*, 22,  
1068 14987-15019, 10.5194/acp-22-14987-2022, 2022.

1069 Wetherbee, G. A., and Mast, M. A.: Annual variations in wet-deposition chemistry related to changes in  
1070 climate, *Clim. Dyn.*, 47, 3141-3155, 10.1007/s00382-016-3017-7, 2016.

1071 Wexler, A. S., and Seinfeld, J. H.: The distribution of ammonium salts among a size and composition  
1072 dispersed aerosol, *Atmospheric Environment. Part A. General Topics*, 24, 1231-1246,  
1073 [https://doi.org/10.1016/0960-1686\(90\)90088-5](https://doi.org/10.1016/0960-1686(90)90088-5), 1990.

1074 Wexler, A. S., and Seinfeld, J. H.: Analysis of aerosol ammonium nitrate: departures from equilibrium  
1075 during SCAQS, *Atmospheric Environment. Part A. General Topics*, 26, 579-591,  
1076 [https://doi.org/10.1016/0960-1686\(92\)90171-G](https://doi.org/10.1016/0960-1686(92)90171-G), 1992.

1077 Xiao, H., Chen, T., and Zhang, Q. et al.: Changes in the dominant contributions of nitrate formation and  
1078 sources during haze episodes: insights from dual isotopic evidence, *J. Geophys. Res.-Atmos.*, 130,  
1079 e2024JD042175, 10.1029/2024JD042175, 2025.

1080 Yan, C., Tham, Y. J., and Nie, W. et al.: Increasing contribution of nighttime nitrogen chemistry to  
1081 wintertime haze formation in Beijing observed during COVID-19 lockdowns, *Nat. Geosci.*, 16, 975-

1082 981, 10.1038/s41561-023-01285-1, 2023.

1083 Yang, L., Shi, Y., and Luo, L.: Review of emission characteristics of fine particles during coal-fired SCR  
1084 DeNOx process, *Proc. Chin. Soc. Electr. Eng.*, 36, 4342-4348, 10.7666/d.Y2782597, 2016.

1085 Yang, T., Li, H., and Xu, W. et al.: Strong impacts of regional atmospheric transport on the vertical  
1086 distribution of aerosol ammonium over Beijing, *Environ. Sci. Technol. Lett.*, 11, 29-34,  
1087 10.1021/acs.estlett.3c00791, 2024.

1088 Yao, X., Lau, A. P. S., and Fang, M. et al.: Size distributions and formation of ionic species in atmospheric  
1089 particulate pollutants in Beijing, China: 1—inorganic ions, *Atmos. Environ.*, 37, 2991-3000,  
1090 10.1016/S1352-2310(03)00255-3, 2003.

1091 Yao, X., Lee, C. J., and Evans, G. J. et al.: Evaluation of ambient SO<sub>2</sub> measurement methods at roadside  
1092 sites, *Atmos. Environ.*, 45, 2781-2788, 10.1016/j.atmosenv.2011.01.070, 2011.

1093 Yao, X., and Zhang, L.: Chemical processes in sea-salt chloride depletion observed at a Canadian rural  
1094 coastal site, *Atmos. Environ.*, 46, 189-194, 10.1016/j.atmosenv.2011.09.081, 2012a.

1095 Yao, X., and Zhang, L.: Supermicron modes of ammonium ions related to fog in rural atmosphere, *Atmos.*  
1096 *Chem. Phys.*, 12, 11165-11178, 10.5194/acp-12-11165-2012, 2012b.

1097 Yao, X., and Zhang, L.: Causes of large increases in atmospheric ammonia in the last decade across  
1098 North America, *ACS Omega*, 4, 22133-22142, 10.1021/acsomega.9b03284, 2019.

1099 Yao, X., and Zhang, L.: Decoding long-term trends in the wet deposition of sulfate, nitrate, and  
1100 ammonium after reducing the perturbation from climate anomalies, *Atmos. Chem. Phys.*, 20, 721-733,  
1101 10.5194/acp-20-721-2020, 2020.

1102 Yao, X., and Zhang, L.: Identifying decadal trends in deweathered concentrations of criteria air pollutants  
1103 in Canadian urban atmospheres with machine learning approaches, *Atmos. Chem. Phys.*, 24, 7773-  
1104 7791, 10.5194/acp-24-7773-2024, 2024.

1105 Yeganeh, B., Shakerdonyavi, A., Zafarmomen, N., and Taheri, A.: Comprehensive spatiotemporal  
1106 analysis of long-term mobile monitoring for traffic-related particles in a complex urban environment,  
1107 *Atmos. Pollut. Res.*, 102870, 10.1016/j.apr.2025.102870, 2025.

1108 Zaveri, R. A., Easter, R. C., and Singh, B. et al.: Development and evaluation of chemistry-aerosol-  
1109 climate model CAM5-chem-MAM7-MOSAIC: global atmospheric distribution and radiative effects  
1110 of nitrate aerosol, *J. Adv. Model. Earth Syst.*, 13, e2020MS002346, 10.1029/2020MS002346, 2021.

1111 Zhai, S., Jacob, D. J., and Wang, X. et al.: Control of particulate nitrate air pollution in China, *Nat. Geosci.*,  
1112 14, 389-395, 10.1038/s41561-021-00726-z, 2021.

1113 Zhang, L., Vet, R., and Wiebe, A. et al.: Characterization of the size-segregated water-soluble inorganic  
1114 ions at eight Canadian rural sites, *Atmos. Chem. Phys.*, 8, 7133-7151, 10.5194/acp-8-7133-2008, 2008.

1115 Zhang, Q., Wang, Y., and Liu, M. et al.: Wintertime formation of large sulfate particles in China and  
1116 implications for human health, *Environ. Sci. Technol.*, 57, 20010-20023, 10.1021/acs.est.3c05645,  
1117 2023.

1118 Zhang, Z., Li, Y., and Zhang, X. et al.: Review of hazardous materials in condensable particulate matter,  
1119 *Fuel Process. Technol.*, 220, 106892, 10.1016/j.fuproc.2021.106892, 2021.

1120 Zhao, S., Hu, B., and Gao, W. et al.: Effect of the “coal to gas” project on atmospheric NO<sub>x</sub> during the  
1121 heating period at a suburban site between Beijing and Tianjin, *Atmos. Res.*, 241, 104977,  
1122 10.1016/j.atmosres.2020.104977, 2020.

1123 Zhou, M., Nie, W., and Qiao, L. et al.: Elevated formation of particulate nitrate from N<sub>2</sub>O<sub>5</sub> hydrolysis in  
1124 the Yangtze River Delta region from 2011 to 2019, *Geophys. Res. Lett.*, 49, e2021GL097393,  
1125 10.1029/2021GL097393, 2022.

1126 Zhu, Y., Sabaliauskas, K., and Liu, X. et al.: Comparative analysis of new particle formation events in  
1127 less and severely polluted urban atmosphere, *Atmos. Environ.*, 98, 655-664,  
1128 10.1016/j.atmosenv.2014.09.043, 2014.

1129

### 1130 **List of Figures**

1131 **Figure 1.** (a) Annual variations of mass concentrations of f-NO<sub>3</sub><sup>-</sup> and c-NO<sub>3</sub><sup>-</sup> in Edmonton, (b)  
1132 annual variations of mixing ratio of NO<sub>2</sub> in Edmonton and provincial total NO<sub>x</sub> emissions, (c) f-  
1133 NO<sub>3</sub><sup>-</sup> and c-NO<sub>3</sub><sup>-</sup> at S-90130 vs. NO<sub>x</sub> emissions, (d) f-NO<sub>3</sub><sup>-</sup> and c-NO<sub>3</sub><sup>-</sup> in Winnipeg, (e) NO<sub>2</sub> mixing  
1134 ratio in Winnipeg and provincial total NO<sub>x</sub> emissions, and time series of 24-h integrated f-NO<sub>3</sub><sup>-</sup> and  
1135 c-NO<sub>3</sub><sup>-</sup> in 1996 (f) and 2007 (g) at a time resolution of one sample in every three days. Blue and  
1136 black markers in (a) represent data obtained at S-90130 and S-90132 in Edmonton, respectively.  
1137 Blue and black markers in (d) represent data points in Winnipeg before and after 2003, respectively.  
1138 Dashed lines in (c) denote least-squares regression fits for f-NO<sub>3</sub><sup>-</sup> and c-NO<sub>3</sub><sup>-</sup>.

1139 **Figure 2.** (a) Annual variations of mass concentrations of f-NO<sub>3</sub><sup>-</sup> and c-NO<sub>3</sub><sup>-</sup> in Quebec City, (b)  
1140 annual variations of mixing ratio of NO<sub>2</sub> in Quebec City and provincial total NO<sub>x</sub> emissions, (c) f-  
1141 NO<sub>3</sub><sup>-</sup> and c-NO<sub>3</sub><sup>-</sup> in Montreal, (d) NO<sub>2</sub> mixing ratio in Montreal, (e) f-NO<sub>3</sub><sup>-</sup> and c-NO<sub>3</sub><sup>-</sup> in Victoria,  
1142 (f) NO<sub>2</sub> mixing ratio in Victoria, (g) f-NO<sub>3</sub><sup>-</sup> and c-NO<sub>3</sub><sup>-</sup> in Vancouver, and (h) NO<sub>2</sub> mixing ratio in  
1143 Vancouver. Blue and black markers in (a) represent data points before and after 2003, respectively.  
1144 Blue and black markers in (c), (e), and (g) represent data points before and after 2002, respectively.

1145 **Figure 3.** Single-factor (T, WS, RH, and HNO<sub>3gas</sub><sup>\*</sup>) effects on daily f-NO<sub>3</sub><sup>-</sup> (and HNO<sub>3</sub><sup>\*</sup> in the case  
1146 of T factor) in 2010 and 2015.

1147 **Figure 4.** Time series of 24-h integrated f-NO<sub>3</sub><sup>-</sup> in 2010 (a) and 2015 (b) in Edmonton at a time  
1148 resolution of one sample in every three days, and correlations in the re-constructed f-NO<sub>3</sub><sup>-</sup> between  
1149 2015 and 2010 using data points with values of full range (0<sup>th</sup>-100<sup>th</sup> percentiles) (c), central 50%  
1150 (25<sup>th</sup>-75<sup>th</sup> percentile) (d), and lower 50% (0<sup>th</sup>-50<sup>th</sup> percentile) (e).

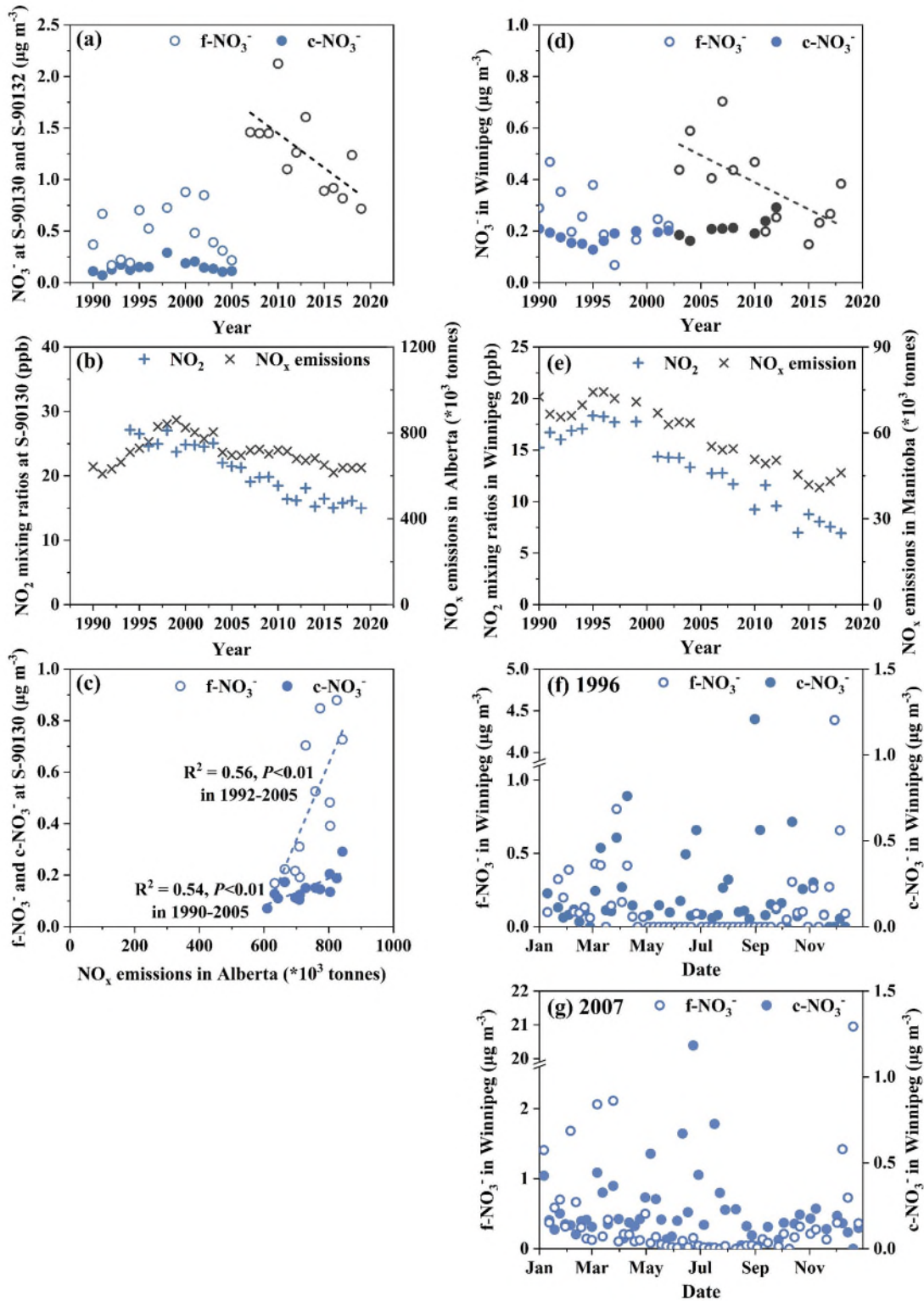


**Figure 1.** (a) Annual variations of mass concentrations of f-NO<sub>3</sub><sup>-</sup> and c-NO<sub>3</sub><sup>-</sup> in Edmonton, (b) annual variations of mixing ratio of NO<sub>2</sub> in Edmonton and provincial total NO<sub>x</sub> emissions, (c) f-NO<sub>3</sub><sup>-</sup> and c-NO<sub>3</sub><sup>-</sup> at S-90130 vs. NO<sub>x</sub> emissions, (d) f-NO<sub>3</sub><sup>-</sup>

and c-NO<sub>3</sub><sup>-</sup> in Winnipeg, (e) NO<sub>2</sub> mixing ratio in Winnipeg and provincial total NO<sub>x</sub> emissions, and time series of 24-h integrated f-NO<sub>3</sub><sup>-</sup> and c-NO<sub>3</sub><sup>-</sup> in 1996 (f) and 2007 (f) at a time resolution of one sample in every three days. Blue and black markers in (a) represent data obtained at S-90130 and S-90132 in Edmonton, respectively. Blue and black markers in (d) represent data points in Winnipeg before and after 2003, respectively. Dashed lines in (c) denote least-squares regression fits for f-NO<sub>3</sub><sup>-</sup> and c-NO<sub>3</sub><sup>-</sup>.

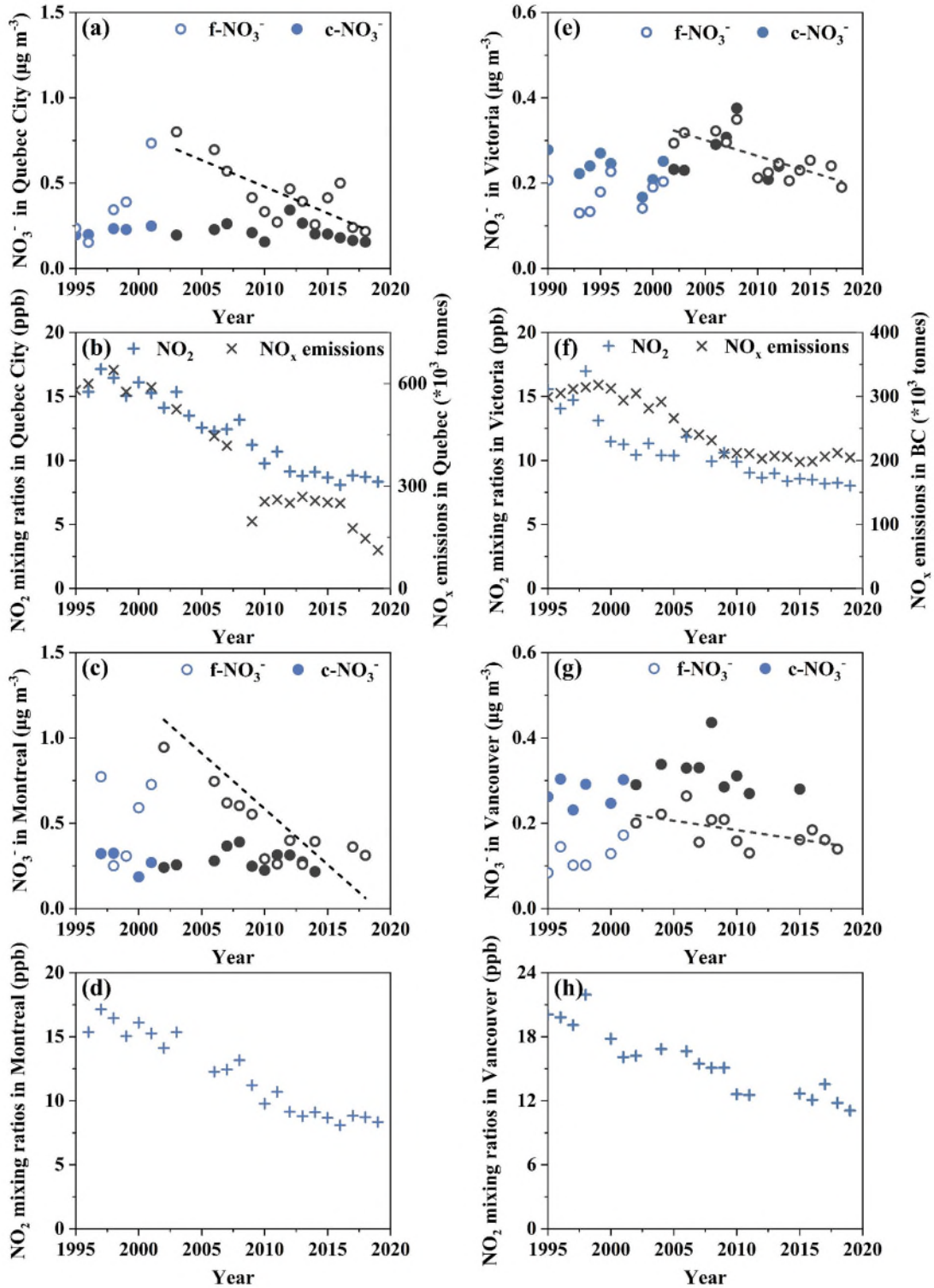


**Figure 2.** (a) Annual variations of mass concentrations of f-NO<sub>3</sub><sup>-</sup> and c-NO<sub>3</sub><sup>-</sup> in Quebec City, (b) annual variations of mixing ratio of NO<sub>2</sub> in Quebec City and provincial total NO<sub>x</sub> emissions, (c) f-NO<sub>3</sub><sup>-</sup> and c-NO<sub>3</sub><sup>-</sup> in Montreal, (d) NO<sub>2</sub> mixing ratio in Montreal, (e) f-NO<sub>3</sub><sup>-</sup> and c-NO<sub>3</sub><sup>-</sup> in Victoria, (f) NO<sub>2</sub> mixing ratio in Victoria, (g) f-NO<sub>3</sub><sup>-</sup> and c-

$\text{NO}_3^-$  in Vancouver, and (h)  $\text{NO}_2$  mixing ratio in Vancouver. Blue and black markers in (a) represent data points before and after 2003, respectively. Blue and black markers in (c), (e), and (g) represent data points before and after 2002, respectively.

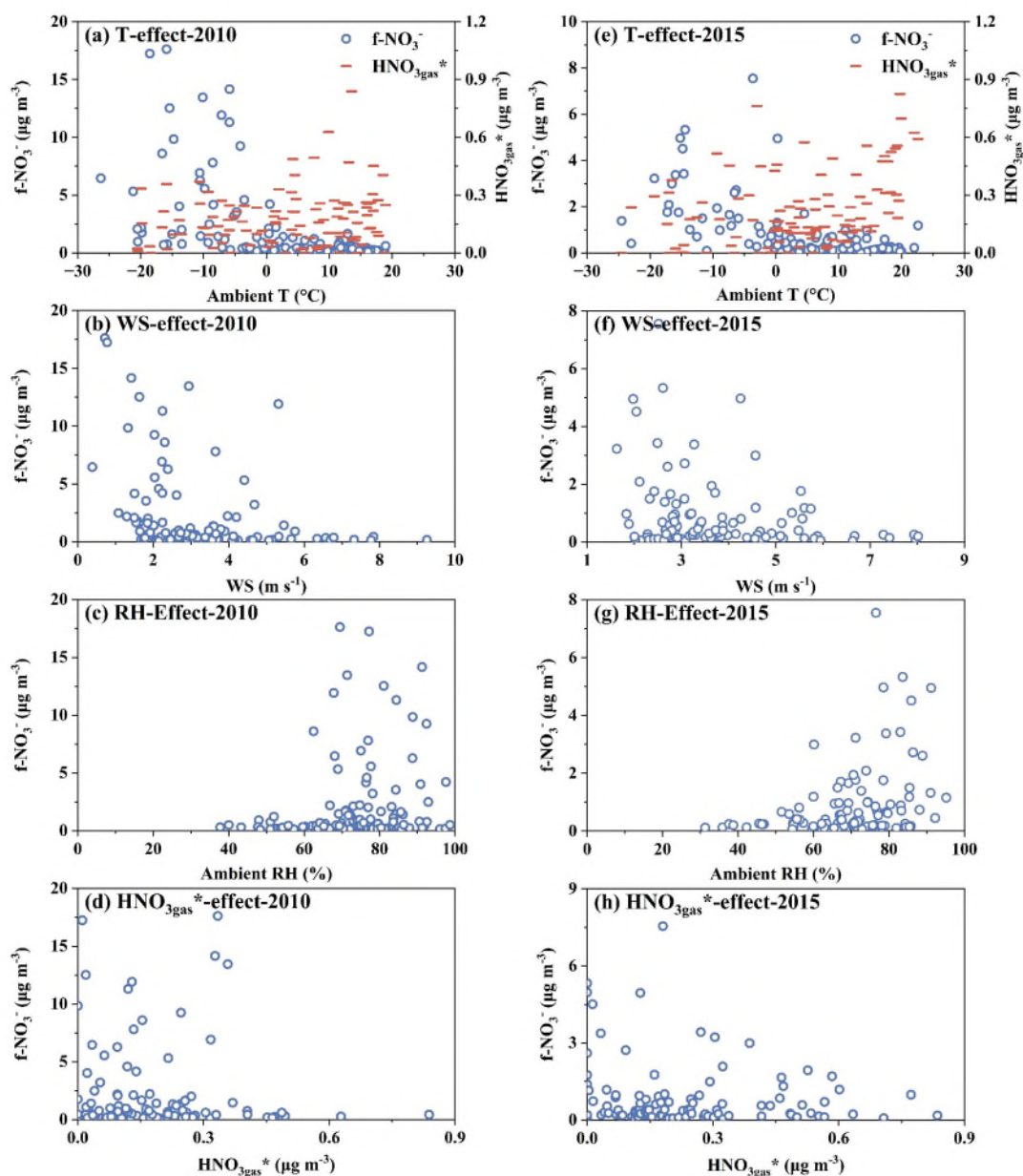


**Figure 3.** Single-factor (T, WS, RH, and  $\text{HNO}_{3\text{gas}}^*$ ) effects on daily  $\text{f-NO}_3^-$  (and  $\text{HNO}_3^*$  in the case of T factor) in 2010 and 2015.

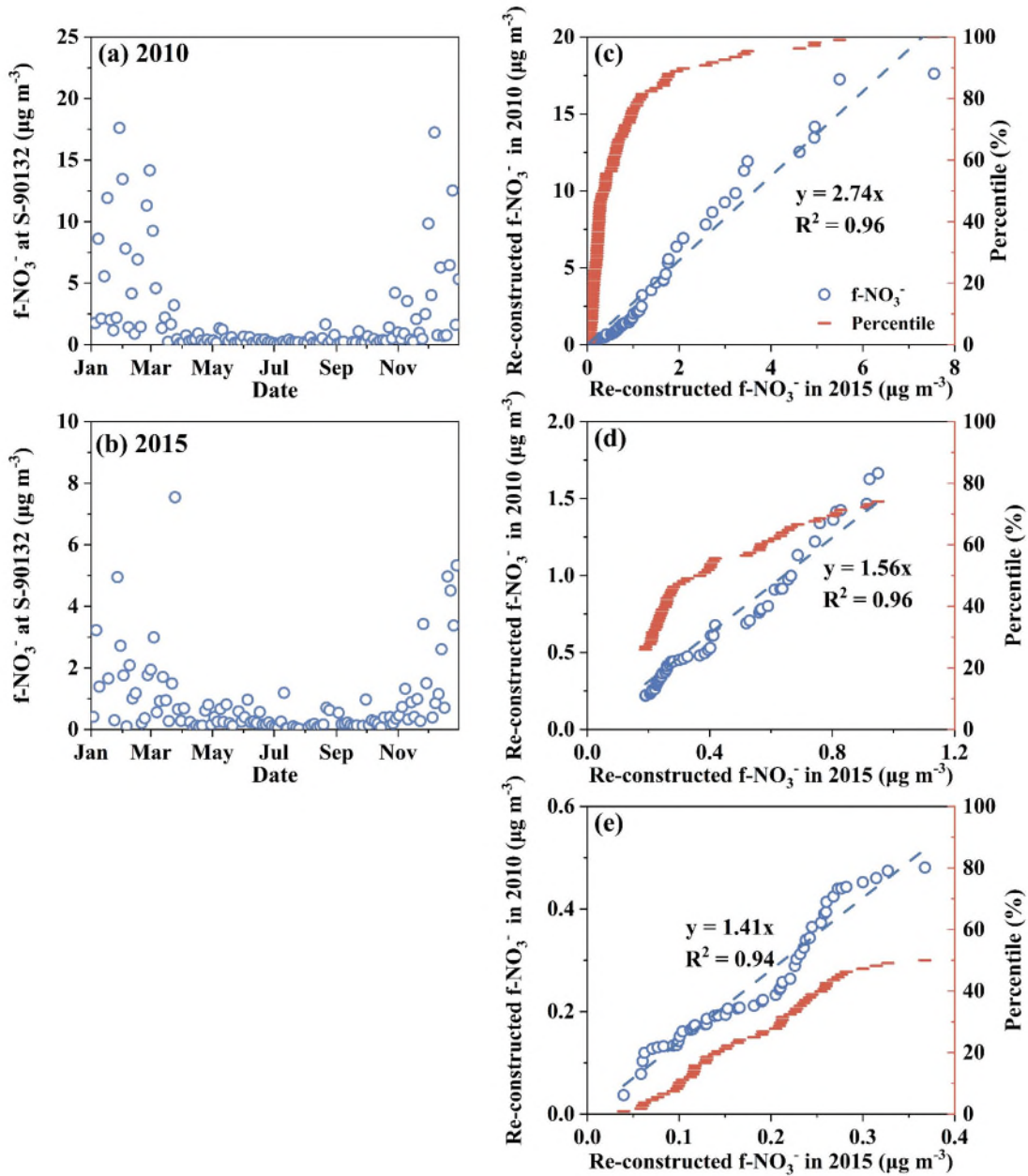


**Figure 4.** Time series of 24-h integrated f-NO<sub>3</sub><sup>-</sup> in 2010 (a) and 2015 (b) in Edmonton at a time resolution of one sample in every three days, and correlations in the re-constructed f-NO<sub>3</sub><sup>-</sup> between 2015 and 2010 using data points with values of full range (0<sup>th</sup>-100<sup>th</sup> percentiles) (c), central 50% (25<sup>th</sup>-75<sup>th</sup> percentile) (d), and lower 50% (0<sup>th</sup>-50<sup>th</sup> percentile) (e).